Spectrally phase-coded O-CDMA [Invited]

Andrew M. Weiner,* Zhi Jiang, and Daniel E. Leaird

School of Electrical and Computer Engineering, Purdue University, West Lafayette, Indiana 47907-2035, USA
**Corresponding author: amw@ecn.purdue.edu*

Received January 18, 2007; accepted April 11, 2007;
published May 21, 2007 (Doc. ID 78880)

A summary of recent progress in our spectrally phase-coded O-CDMA system is presented, including multiuser ~Gbits/s system demonstrations, error-free ultrafast fiber transmission over 50 km single-mode fiber with ~500 fs pulses, code translation demonstrations as may be required in a multipoint network implementation, and experimental studies of potential security issues in O-CDMA. © 2007 Optical Society of America

OCIS codes: 060.2330, 320.7160.

1. Introduction

Multiple access techniques are required in order to meet the demand for high-speed and large-capacity communications in optical networks allowing multiple users to share the fiber bandwidth. There are three major multiple access approaches: each user is allocated a specific time slot in time-division multiplexing (TDM), and a specific frequency (wavelength) slot in wavelength-division multiplexing (WDM). Both techniques have been extensively explored and utilized in optical communication systems [1,2]. Alternatively, optical code-division multiple access (O-CDMA) [3–29] is receiving increasing attention due to its simplified and decentralized network control, potential improved spectral efficiency, soft-limited capacity, and increased flexibility in the granularity of bandwidth that can be provisioned. In O-CDMA, different users whose signals may be overlapped both in time and frequency share a common communications medium; multiple access is achieved by assigning different, minimally interfering code sequences to different CDMA transmitters, which must subsequently be detected in the presence of multiaccess interference (MAI) from other users. Figure 1 shows a schematic of bandwidth allocation in TDM, WDM, and O-CDMA.

CDMA derives from radio frequency (rf) spread spectrum communications, originally developed for military applications due to an inherent low probability of intercept and immunity to interference, and more recently for commercial rf cellular radio applications [30,31]. CDMA is now becoming the dominant multiple access technique in rf wireless networks. Since rf-CDMA works with typical carrier frequencies in the ~1 GHz range and bit rates of the order of ~100 kbits/s, current electronic technologies can easily provide coding techniques and long temporal codes (~1000 chips) for each bit, which is critical to support a large number of potential users [3]. In addition, the system bit error rate (BER) requirement is usually not so strict for rf-CDMA. In contrast, the need to perform encoding and decoding for O-CDMA poses one immediate challenge both because of the optical carrier frequency and the much higher bit rates (multiple Gbits/s per user), which already approaches the limit of electronic processing. Therefore, innovative all-optical processing technologies are needed. In addition, challenges for O-CDMA also come from critical requirements that are routinely required in optical communication systems. These requirements include extreme high quality of service (QoS) (BER at 10^{-9} or below), large capacity (tens or hundreds of users, total capacity up to ~100 Gbits/s or above), and relatively long distance transmission [kilometers to ~100 km for local area networks (LAN) and metropolitan area networks (MAN)]. Although the raw BER requirements for O-CDMA may be relaxed by the use of modern high-speed forward-error-correction technologies, the challenges for O-CDMA implementation remain significant.

Several different O-CDMA schemes have been proposed [3–29], based on different choices of sources, coding schemes, and detection. O-CDMA schemes may generally be classified according to the choice of coherent versus incoherent processing, coherent

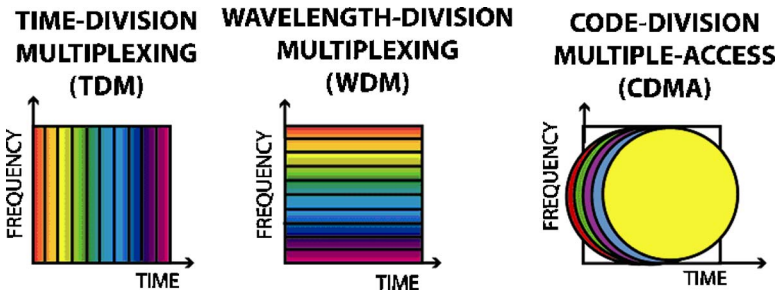

Fig. 1. Schematic of bandwidth allocation in TDM, WDM, and CDMA optical networks.

(mode-locked pulses) versus incoherent [e.g., amplified spontaneous emission (ASE) and light emitting diode (LED)] broadband optical source, and encoding method (time domain versus frequency domain, amplitude versus phase). Schemes based on incoherent processing (summing of optical powers) and broadband incoherent (noise) sources are generally the easiest to implement but offer relatively poor performance. To increase the available coding space, time–wavelength (2-D) coding schemes have been proposed [15,16], where each code chip corresponds to a specific time position and wavelength position within a bit as determined by a code matrix. This scheme may utilize either coherent or incoherent sources but employs incoherent processing (summing of optical powers from chips with different wavelength and time positions). Note that fundamentally, when different optical sources are superimposed, it is the complex field amplitudes (not power) that adds. To reach the incoherent processing limit based on the addition of power, each time–wavelength cell in the 2-D code matrix must itself be incoherent, i.e., significantly exceed the bandwidth limit. This requirement, which seriously constrains spectral efficiency, has received little attention in the literature.

As in radio spread spectrum systems, coherent processing based on manipulation of optical fields, which can be made to sum to zero, is required for strongest suppression of MAI and for enhanced performance. Coherent O-CDMA using both a coherent source (mode-locked laser) and coherent processing promises increased performance and has recently attracted intensive experimental investigations. The encoding–decoding process can be implemented in either the time domain or frequency domain. The first coherent O-CDMA scheme to be introduced was the frequency domain approach [5,6]. In this spectrally phase coded O-CDMA scheme, short pulses from a mode-locked laser are spectrally dispersed in space, and a spatial light modulator is used to apply appropriate phases onto different spectral chips. As a consequence of this spectral coding process, pulses are spread in time, usually in a pseudorandom manner. Due to the use of the spatial light modulator, this approach to encoding is inherently programmable. Spectral phase coded O-CDMA has been investigated by many groups [5–10,21–29]. In the temporally phase coded O-CDMA scheme, short pulses from mode-locked laser are spread directly in time, and appropriate phases are then imposed onto different temporal chips [11,12,17–19]. Both superstructured fiber Bragg gratings (SSFBGs) and transversal filters implemented in planar light wave circuit technology have been used to implement the encoding function. Generally the SSFBGs support long code lengths but are fixed, while transversal filters support only short code lengths but may be programmable. In both the frequency- and time-domain approaches, the job of the decoder is to apply a conjugate phase function (either in frequency or time, respectively), which restores the O-CDMA signal to its initial ultrashort pulse character.

O-CDMA performance has been analyzed theoretically both for spectral [6] and temporal [20] phase coding schemes. Although we are not aware of any direct comparison of the theoretical performance of these approaches, both analyses point to a number of common features:

(1) Performance is governed by the ability to reject interference generated by other noncoordinated users. Such interference includes both those portions of the interfering users overlapped in time with a decoded short pulse signal and those portions not overlapped in time. In [6] both forms of interference are designated MAI, while in [20] MAI denotes only the nontemporally overlapped interference and the term signal-interference (SI) beat noise is used to denote the temporally overlapped interference.

Nevertheless, both theories fully account for both types of interference. The temporally overlapped interference, or SI beat noise, is generally the more serious interference term. In this paper we generally use MAI to refer to both types of interference.

(2) For a given code length, BER performance degrades with increasing number of noncoordinated users. Hence there is a soft-limited trade-off between user count and error-rate performance.

(3) Code length is very important. For a given number of users, increased code length allows significantly better suppression of interference and significantly lower error rate. Conversely, with increased code length a significantly higher user count can be supported at fixed error rate.

(4) Without coordination between users (i.e., full asynchronism in time and full spectral overlap) and without error correction, O-CDMA is not a high-spectral-efficiency technique.

At present only temporally phase-encoded O-CDMA has been operated in a truly asynchronous and spectrally overlapped manner at bit rates in the Gbits/s range [17]. This is made possible mainly due to ultralong code length using 511 chip SSFBG encoders and decoders, which allows excellent interference suppression. On the other hand, this encoder–decoder technology is not programmable, and the very long code length hinders high-individual-user bit rates. Spectral phase encoding offers full programmability, but to date has provided comparatively shorter codes (e.g., length 31 is typical). For this reason some form of timing coordination is generally employed in order to obtain good error rate performance in spectrally phase-coded O-CDMA experiments. One early two user, spectral phase coded O-CDMA experiment performed at low bit rate did demonstrate full asynchronism [8]. We will discuss timing coordination in detail below. In addition to programmability, spectral phase coding allows a simple path to code translation, which we will also discuss later. In this paper we will focus on the spectral phase-coding approach, and, in particular, on recent experimental progress in spectral phase-coded O-CDMA in our laboratory at Purdue University.

Briefly, we comment also on one additional set of experiments that has been classified as O-CDMA [32,33]. In these experiments short pulses are coupled into an arrayed waveguide grating (AWG), with the pulse bandwidth exceeding the AWG free spectral range. As shown in [34–36], the output in this case consists of a temporally periodic spaced pulse burst. The output spectrum consists of a periodic burst of narrow spectral peaks, separated by the free spectral range of the AWG. Furthermore, at different output guides of the AWG, the bursts of spectral peaks are shifted by an amount equal to the AWG channel spacing (this typically exceeds the linewidth of the individual peaks). In [32,33] AWGs are used in this mode as encoders and decoders, and provide strong suppression of nonmatched waveforms. Here we argue that this suppression occurs because the different output "codes" have little spectral overlap with each other (when viewed with sufficiently high spectral resolution), as would also be true for different AWG outputs in a conventional WDM system. Because the different waveforms are ideally orthogonal in frequency, this approach is quite different than other O-CDMA schemes considered here. Although certainly interesting, we propose that such experiments [32,33] are better classified as a novel type of WDM. As such, the capacity is likely hard limited, rather than soft limited, as is expected for O-CDMA.

Our ultrashort pulse O-CDMA scheme based on spectral phase encoding has an interesting analogy with the most widely used direct sequence (DS) rf-CDMA. Figure 2 shows time- and frequency-domain evolution during encoding and decoding for these two schemes. For DS rf-CDMA, a bit is divided into many temporal chips and phase coded for each chip [for example, 0 or π phase shift for binary phase-shift keying (BPSK)] in the time domain [Fig. 2(A)], so that the spectrum of a narrowband signal is broadened during the encoding process [Fig. 2(B)]. After decoding at the receiver, a properly decoded signal is recovered back to a narrowband signal, which can be separated out by a narrowband filter from the improperly decoded broadband MAI. This encoding–decoding process manifests the spread spectrum property of DS rf-CDMA [30,31] where there exists a trade-off between bandwidth and performance. Our O-CDMA scheme is just a time-frequency reversed version of DS rf-CDMA, where the ultrashort pulse spectrum is divided to many frequency chips and phase coded for each chip [Fig. 2(A)]. This results in spreading in the time domain [Fig. 2(B)], while proper decoding despreads the encoded signal back to its original duration in time.

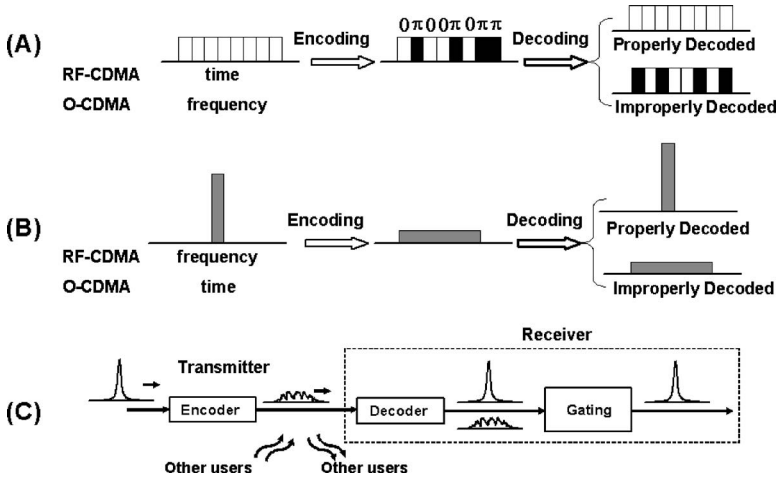

Fig. 2. Comparison of direct sequence RF-CDMA and spectral phase coded O-CDMA. (A) Time-domain behavior for RF-CDMA (equivalent to frequency-domain behavior for O-CDMA). (B) Frequency-domain behavior for RF-CDMA (equivalent to time-domain behavior for O-CDMA). (C) Conceptual diagram of an O-CDMA network. The gating function can be implemented: (1) frequency gating (narrow bandpass filter) in RF-CDMA, (2) real-time gating in O-CDMA,[11,12,21–25] (3) self-time gating by nonlinear optics in our O-CDMA.

Figure 2(C) shows the conceptual O-CDMA network diagram for many of the O-CDMA approaches using ultrashort pulses. Input ultrashort pulses are time spread during the encoding process into lower intensity noiselike signals [5–12,17–29]. In the receiver, data corresponding to a desired user is separated from MAI via a matched filtering (decoding) operation, in which properly decoded signals are converted back to the original pulselike signals, while improperly decoded signals remain low-intensity noiselike temporally broad waveforms. Since the energy in properly and improperly decoded signals remains similar, and since the temporal duration of even improperly decoded signals is on the order of the bit period or below, both properly and improperly decoded signals will appear essentially identical to an electronic receiver band-limited to the data rate. Consequently either very fast electronics or an optical gating function play a critical role in separating properly decoded short pulses from improperly decoded MAI.

In rf-CDMA, the gating process can be implemented easily in the frequency domain, where a narrow bandpass filter is used. In O-CDMA, the gating has to be implemented in the time domain on an ultrafast time scale (comparable with the mode-locked pulse duration), which is not trivial. In our system, a nonlinear optical intensity discriminator provides a self-gating functionality that enables asynchronous detection. Optical gating via a separate stream of optical control pulses has also been used extensively in spectrally phase-coded O-CDMA [21–25]. This approach offers good performance but imposes stricter synchronism requirements. An important issue is that in a real system, synchronous optical gating requires clock recovery. Figure 3(A) depicts a system employing gating with conventional data modulation, as

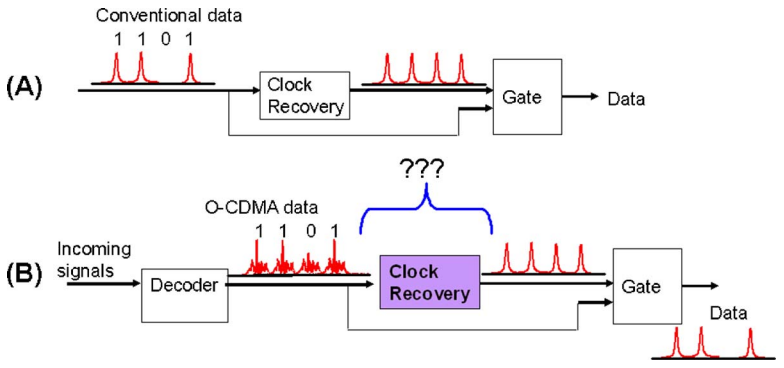

Fig. 3. Clock recovery for optical gating in (A) conventional data and (B) O-CDMA data.

in a high-speed time-division demultiplexer, where the clock recovery can be achieved from the incoming data stream [37]. Figure 3(B) shows the situation in O-CDMA. Since the incoming data stream includes both properly decoded and improperly decoded users, they are not distinguishable (using a detector with bandwidth limited to the data rate) prior to timing gating. Furthermore, the overlap of multiple data streams may also result in a serious noise process (see Section 5). Both issues are expected to seriously hinder clock recovery for the properly decoded user. This causes a dilemma: clock recovery requires time gating first to separate out the properly decoded user, while time gating requires clock recovery first for synchronized operation. To our knowledge true clock recovery in the presence of multiple overlapping phase-coded O-CDMA users has not yet been demonstrated and remains a serious challenge for practical application of synchronous gating in phase-coded O-CDMA. Consequently, in our research we employ a self-gating approach via nonlinear optics, which avoids the O-CDMA clock recovery problem by employing asynchronous detection.

In addition to the synchronism issues on the detection side, there are also synchronism issues on the transmitter side in O-CDMA. CDMA is well-suited to bursty network environments, and the asynchronous nature of data transmission can simplify and decentralize network management and control. However, due to O-CDMA system requirements mentioned above, full asynchronism is difficult to implement in practice while simultaneously maintaining sufficient MAI suppression. Therefore, some level of synchronism is built into many $\geqslant$ two-user O-CDMA schemes, and in particular to most studies employing spectral phase coding. The time scales relevant for a discussion of synchronism requirements are illustrated in Fig. 4. The coarsest time scale is the bit period, t_{bit}. Uncoded or properly decoded waveforms have a duration that is called the chip duration, t_{chip}. Encoded or improperly decoded pulses are pseudonoise waveforms with a larger duration, which we refer to as the slot duration t_{slot}. In our spectral phase-coded O-CDMA scheme, the individual features in the pseudonoise waveforms have characteristic durations equal to t_{chip}, and the number of independent features is equal to the code length N, i.e., $t_{\text{slot}}/t_{\text{chip}}=N$. Fully asynchronous system signals transmitted by any user can fall anywhere within a bit duration t_{bit} without coordination with other users. In a fully synchronous system, the signal transmitted by any specific user must be coordinated with the transmission time of all the other users, with a timing precision below t_{chip}. Furthermore, a synchronous receiver would require optical clock recovery for gating with timing precision also below t_{chip}. To relax the timing requirements of the fully synchronous approach, in some of our work we have proposed the concept of slot-level coordination: the transmission time of a user is controlled on the time scale of the slot duration t_{slot}, but without the need for chip-level timing control [26–28]. Accordingly, O-CDMA can be classified according to different levels of synchronism requirements. At the transmitter side, we distinguish between no timing coordination (full asynchronism), slot-level (t_{slot}) coordination, and chip-level (t_{chip}) coordination. At the receiver side, we distinguish between asynchronous detection and synchronous detection requiring chip-level (t_{chip}) precision (either using ultrafast electronics or optical gating with clock recovery). All the possible combinations are listed in Table 1 with representative references. It is clear that chip-level transmission coordination and/or synchronous detection requiring chip-level (t_{chip}) speed are used in many multiple-user O-CDMA schemes. This sacrifices one of the most significant advantages, asynchronism, of CDMA. As mentioned earlier, truly asynchronous operation has been demonstrated recently using a fixed encoder–decoder technology supporting an ultralong code length [17]. Our scheme only requires slot-level timing coordination at the transmitter; fully asynchronous detection is achieved by means of a novel, asynchronous nonlinear optical processing technique. Slot-level timing coordination has also been adopted in some experiments by other O-CDMA groups [21–23]. In this paper, we will discuss experiments with slot-level coordination as well as experiments with chip-level coordination at the transmitter, but always with asynchronous detection at receiver.

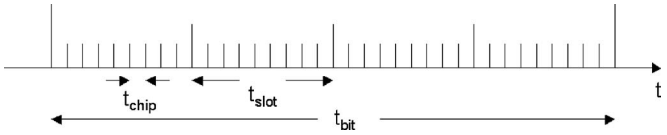

Fig. 4. Timing control in O-CDMA optical networks.

Table 1. Comparison of O-CDMA Schemes in Terms of Timing Requirement (TR)

	Transmitter Requirement					
Receiver Requirement	No Coordination	Ref.	Slot-Level Coordination	Ref.	Chip-Level Coordination	Ref.
Asynchronous detection	TR: low	[8,17]	TR: medium	[26–28]	TR: high	[29]
Synchronous detection requiring chip level (t_{chip}) speed	TR: high	—	TR: high	—	TR: high	[11,12,21–25]

The remainder of this paper is structured as follows. In Section 2, we describe a testbed for multiple-user, spectrally phase-coded O-CDMA and system studies at 10 Gbits/s per user. Our testbed is based on pulse shapers as encoders and decoders and an ultrasensitive nonlinear optical intensity discriminator (thresholder) based on second-harmonic generation (SHG) in a periodically poled lithium niobate (PPLN) waveguide. Our nonlinear discriminator permits full MAI suppression at an operating energy of ~30 fJ/bit, as much as 2 orders of magnitude lower than previous discriminators based on nonlinear fiber optics [7,8,19,22].

In subsequent sections we discuss several additional experiments relevant to O-CDMA. In Section 3 we discuss dispersion compensation for fiber transmission of short pulses [38–43]. We are able to demonstrate essentially distortionless 50 km fiber transmission for ~500 fs pulses. Such dispersion-compensated transmission is critical for ultrafast O-CDMA system using ultrashort pulses for applications in LANs as well as MANs.

In Section 4 we discuss code translation in O-CDMA networks [44–49]. In particular, we experimentally demonstrate reconfigurable all-optical code translation in spectrally phase-coded O-CDMA. Code translation may permit the resolution of code conflicts, increase user counts, and reduce the number of required codes through code reuse. The ability to dynamically translate from one code to another in an O-CDMA network is analogous to dynamic wavelength conversion or switching, which is a key capability for reconfigurable wavelength-division-multiplexed networks.

In Section 5 we discuss security issues in O-CDMA [50–54]. The potential provided by O-CDMA for enhanced information security via physical layer encoding is frequently mentioned in addition to other possible advantages. This is plausible at first glance considering that frequently the O-CDMA encoded signal manifests itself as a noiselike waveform that may not be accessible to an eavesdropper without knowledge of the applied code. Therefore, for a properly configured system, an eavesdropper may potentially experience a significant disadvantage in signal-to-noise ratio compared to the authorized O-CDMA receiver. However, to explore this argument more deeply, we have performed experimental studies of various security issues in O-CDMA [52,53]. Here we discuss our experiments of security using a code switching scheme as well as new results using a multiple-user aggregation scheme. In both cases we demonstrate vulnerabilities that may permit an eavesdropper to recover data from these schemes. Our results show that there may be opportunities for exploiting structure in coded O-CDMA signals in order to eavesdrop, without the need to measure and determine the code, or in some cases to determine the codes without the need for highly sophisticated hardware. Therefore, one needs to exercise great care in assessing and mitigating such vulnerabilities if the physical-layer security features of O-CDMA are of interest. In Section 6 we conclude.

2. Multiuser ~Gbits/s System Demonstration

We have performed O-CDMA system studies with up to four users at 10 Gbits/s, both with slot-level timing coordination and with a combination of chip- and slot-level timing coordination. We first discuss the slot-level experiments.

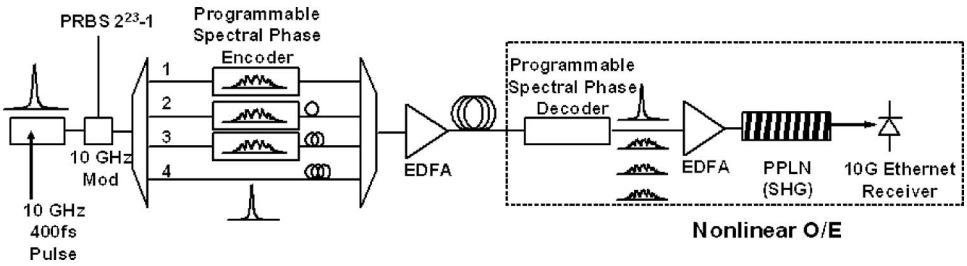

Fig. 5. Four-user O-CDMA system testbed.

2.A. Slot-Level Timing Coordination O-CDMA System

We have demonstrated a four-user, 2.5 Gbits/s and four-user 10 Gbits/s O-CDMA system with slot-level timing coordination and asynchronous detection with ultralow optical power (30 fJ/bit) [26–28]. Here we summarize our 10 Gbits/s results. A schematic of the four-user, 10 Gbits/s O-CDMA demonstration is shown in Fig. 5. An actively mode-locked fiber laser followed by a dispersion decreasing fiber soliton compressor producing nearly transform-limited ~0.4 ps pulses at 10 GHz centered near 1542 nm is used as the pulse source. A 10 Gbits/s pseudorandom binary sequence (PRBS) $2^{23}-1$ data stream is impressed upon pulses. For three users, the modulated ultrashort pulses are input into fiber-coupled Fourier-transform pulse shapers [55] to spectrally phase code the spectrum of the source laser. A fourth uncoded user path is also present as an additional interference channel [26]. The receiver consists of a fiber-coupled Fourier-transform pulse shaper used to select the user channel to decode, an optical amplifier, a highly sensitive fiber pigtailed PPLN waveguide chip to perform the nonlinear discrimination function [56], and a 10 Gbits/s Ethernet photoreceiver (3 dB bandwidth of 7.5 GHz), operating at the second-harmonic wavelength of 0.77 μm.

Both encoding and decoding are implemented by the well-developed ultrashort pulse shaping techniques using a fiber-coupled Fourier-transform pulse shaper that incorporates a 2×128 pixel liquid-crystal modulator (LCM) array to spectrally phase code the spectrum of the source laser. The individual pixels of the LCM can be electronically controlled independently to give an arbitrary phase shift in the range of 0 to 2π with 12-bit resolution [26–29]. Discrete frequency components making up the input short pulse are horizontally diffracted by a grating and programmably controlled by the LCM. Other spectral phase encoding–decoding devices are also available now, including AWG [10] and ring resonators [24,25]. To summarize, the encoding–decoding technologies in literature and their key attributes are listed in Table 2.

As mentioned in the Introduction, a nonlinear optical intensity discriminator plays a critical role in separating properly decoded short pulses from improperly decoded

Table 2. Comparison of O-CDMA Encoding and Decoding Technologies

	Frequency Domain Coding O-CDMA			Time Domain Coding O-CDMA	
	Devices				
	Pulse Shaper	Ring Resonator	AWG[a]	TVF[b]	FBG[c]
References	[22,26,27]	[25]	[10]	[11]	[13,17]
Programmability	Yes	Yes	No	Yes	No
Compactness	Bulk	Integrated	Integrated	Integrated	Integrated
Code length	32–128	8	255[d]	3	64, 511
Loss (dB)	4	4	NA[e]	NA	NA

[a]AWG, Array waveguide grating.

[b]TVF, transversal filter.

[c]FBG, fiber Bragg grating.

[d]This represents the number of phase chips on the pulse shaping mask, which apparently were resolved only in part by the optical apparatus.

[e]NA, not available.

MAI. In our testbed, successful information recovery from MAI is achieved by the use of an ultrasensitive nonlinear optical intensity discriminator based on SHG in a PPLN waveguide. The PPLN chip is 67 mm long with 62 mm periodically poled and a channel waveguide fabricated by reverse proton exchange [56]. The propagation losses were 0.2 dB/cm. The PPLN waveguide SHG phase-matching spectrum exhibits a sinc^2 shape with 0.17 nm bandwidth centered at 1542 nm by temperature tuning to 92.5°C. Its center wavelength shifts ~0.1 nm/°C, with almost the same profile. The phase-matching bandwidth is consistent with 18.6 ps temporal walk-off between the fundamental and SHG fields. The measured internal SHG efficiency at the peak of the phase-matching curve is 3100%/W for continuous wave (cw) and 170%/pJ for ultrashort pulses. The use of a waveguide structure together with a long nonlinear medium leads to dramatically increased SHG conversion efficiency for uncoded or properly decoded (bandwidth limited) pulses; on the other hand, SHG can be strongly suppressed for spectral phase-encoded or improperly decoded pulses. More precisely, one can control the SHG yield by changing the correlation properties of the applied spectral phase-code sequences [57,58]. In this way, the ability to discriminate between uncoded (properly decoded) and encoded (improperly decoded) pulses is greatly enhanced. As a result, second-harmonic power contrast ratios of up to 20.1 dB between uncoded and encoded waveforms were observed when coding with a length-31 MS code in experiments at 10 GHz [59].

Our nonlinear discriminator permits full MAI suppression at an operating energy of ~30 fJ/bit, as much as 2 orders of magnitude lower than previous discriminators based on nonlinear fiber optics [7,8,19,22]. The ability to operate at low power per user is critical for scaling an O-CDMA system to multiple users. A PPLN waveguide device has subsequently been adopted as an optical thresholder for time domain O-CDMA studies [18]. In that work the device works in difference frequency generation (DFG) mode with the help of a high-power cw pump laser. Although this approach requires higher power, it provides the advantage that the DFG signal is still in the 1.5 μm communication wavelength band that allows more options in receiver technology and other possible optical signal processing operations.

The power scaling issue can be understood as follows. Let us assume that the self-gated nonlinear discriminator key to our scheme requires some value U_{bit} to achieve a desired BER performance, where U_{bit} is the energy required per bit for a single properly decoded user. Since equal samples of each channel are seen by every O-CDMA receiver, the average power required at the nonlinear element is $0.5CBU_{\text{bit}}$, where C is the number of channels, B is the data rate, and the factor 0.5 comes from ON–OFF keying (OOK). Previous demonstrations of O-CDMA nonlinear discriminators were based on nonlinear fiber optics, where typical values for U_{bit} range from 1.6–50 pJ [7,8,19,22]. For four 10 Gbits/s channels, this gives an average power requirement of 18–30 dBm at each receiver. Scaling to significantly higher bit rates and channel numbers would require a very large optical amplifier at each receiver, which is highly undesirable for application to networks with large numbers of nodes. To address this scaling issue, it is critical to reduce U_{bit}. Our experiments using waveguide SHG generation achieve ~30 fJ/bit at 10 Gbits/s, a reduction of 2 orders of magnitude compared to discriminators based on nonlinear fiber optics.

Figure 6(A) shows intensity cross-correlation measurements of uncoded and

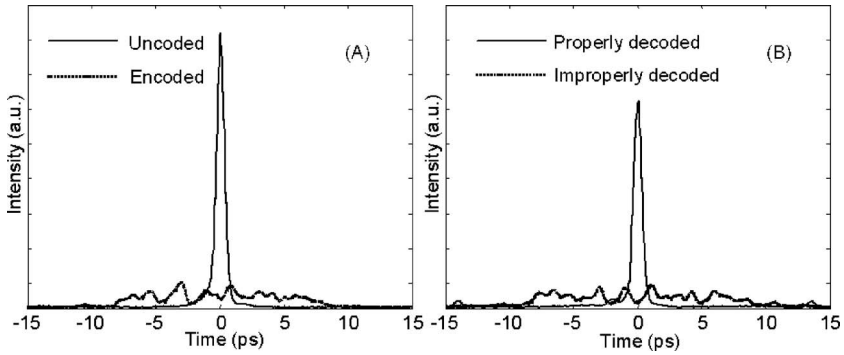

Fig. 6. Intensity cross-correlation measurements. (A) uncoded (solid curve) and 31 MS encoded (dotted curve) pulses. (B) Properly decoded (solid curve) and improperly decoded (dotted curve) pulses.

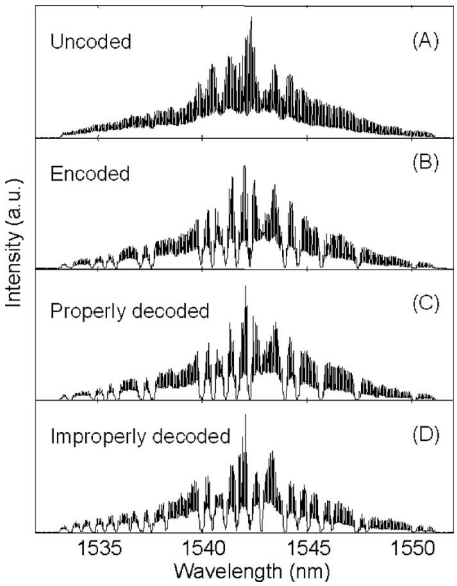

Fig. 7. Optical spectra measurements. (A) Uncoded, (B) 31 MS encoded, (C) properly decoded and improperly decoded. Optical spectrum analyzer (OSA) resolution: 0.05 nm.

encoded waveforms with a length-31 MS code (four LCM pixels per code element). The uncoded short pulse is broadened to an ~20 ps pseudonoise waveform after encoding. Figure 6(B) shows decoded pulses after two shapers forming an encoder–decoder pair. The improperly decoded pulse remains a broadened pseudonoise waveform as MAI. The properly decoded pulse is converted back to a short pulse with 1.4 dB coding loss and minimal side lobes located at ±14.3 ps, which clearly demonstrates successful decoding in the time domain.

Figure 7 shows optical spectra measurement of uncoded, encoded, properly, and improperly decoded pulses corresponding to the time-domain traces shown in Fig. 6. The spectrum for the uncoded pulse in Fig. 7(A) shows ~17.9 nm spectral coding range cut at the edge of the input spectrum. Clear spectral dips are observed in the encoded–decoded spectra in Figs. 7(B)–7(D) whenever a $0-\pi$ phase transition occurs in the spectrum explaining the 1.4 dB coding loss and side lobes mentioned above. The dips in the spectra are related to diffraction effects arising from the frequency components of the input pulse that fall at $0-\pi$ transitions of the LCM in the pulse shaper, which has been quantitatively clarified by simulation and theoretical analysis [7,60]. The properly decoded pulse spectrum in Fig. 7(C) looks very similar to the encoded one in Fig. 7(B) except for slightly wider spectral dips since the dips generated by the encoder and decoder are located exactly at the same position, which clearly shows successful decoding in the frequency domain. Finally, there are more dips on the spectrum of the improperly decoded pulse in Fig. 7(D) because $0-\pi$ transitions between the encoder and decoder are different. Although these spectral dips do not significantly impact our four-user O-CDMA demonstrations, they will play an important role in our discussion of security issues in O-CDMA.

Figure 8 demonstrates the ability to properly decode any of the four-user channels by the correct selection of decoder spectral phase code: here a length-31 *M*-sequence code. The figure shows intensity cross-correlation measurements measured before the nonlinear processor. In this experiment, the pulses from each user are roughly separated by ~25 ps in a time-slotted O-CDMA scheme. There is no need for precise chip-level control of the time offsets. It is interesting to point out that the improperly decoded user has different waveform structures when a different user is properly decoded as shown in the insets. Nonlinear processing enables us to separate the desired user from MAI thereby permitting a multiuser system. As shown before in [26,27], communication requires a nonlinear discriminator, since a data-rate-limited receiver is too slow to resolve the small timing shifts between slots. Figure 9(A) shows the eye diagrams of properly decoded user 1 for one user, two users, and four users. The clean eye diagrams clearly demonstrate the ability to properly decode the desired user and separate it from the MAI. Figure 9(B) shows corresponding BER curves for user 1 plotted versus the total power in the nonlinear discriminator. The ~3 dB power

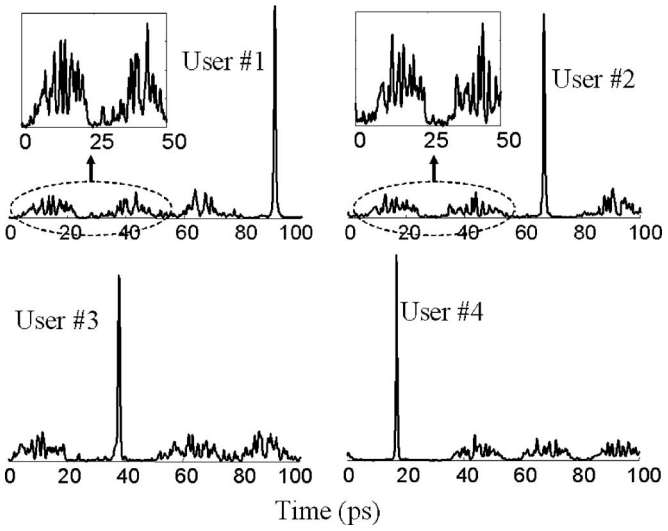

Fig. 8. Intensity cross-correlation measurements of properly decoded channels 1 to 4 demonstrating the ability to selectively decode any of the four-user channels. Channel 4 is the uncoded user. 4×10 Gbits/s system.

differences between BER curves are simply due to the doubling of the number of users. This implies almost negligible power penalty induced by MAI. We can operate with one user at BER$=10^{-9}$ at a power level of less than −5.5 dBm (28.2 fJ/bit), and four users at less than 1 dBm (31.5 fJ/bit), showing significant improvement compared with other approaches utilizing optical fiber nonlinearities. Figure 9(C) shows BER curves for all four users. Even the worst channel, in which we attribute the degradation to the finite interference suppression of the nonlinear discriminator, still operates at BER$=10^{-9}$ with a four-user power of 2 dBm (39.6 fJ/bit). From a system point of view, it is important to run all four users successfully since MAI may exhibit distinct suppression characteristics for each specific desired user. The key points are that we can achieve almost (a) no power penalty and (b) essentially the same performance for all users, both of which are often significant challenges in O-CDMA. In addition, in our system the ~30 fJ/bit requirement provides substantial margin for scaling to higher bit rates and user counts while provisioning only a moderately sized optical amplifier to each receiver node.

We emphasize that our scheme only requires slot-level timing coordination, and nonlinear processing and detection is fully asynchronous. In these experiments we

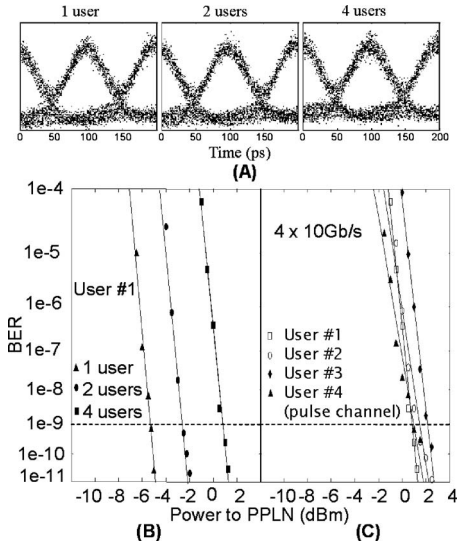

Fig. 9. Performance measurement of the 4×10 Gbits/s O-CDMA system. (A) Eye diagram of properly decoded user 1 for one user, two users, and four users. (B) BER measurements of user 1 corresponding to (A). (C) BER measurement of all four users. Powers refer to the values in the PPLN nonlinear discriminator.

intentionally separated the four users in the time domain (Fig. 8). The system performance is degraded as pulses overlap between users. Figure 10 shows the eye diagrams for a two-user experiment while tuning the separation between the users. Length-31 M-sequence coding is still used such that the interference user is broadened to an ~20 ps pseudonoise waveform. Negligible degradation is observed when the two users separation is 20 and 30 ps. At 10 ps separation the eye diagram becomes noisy. At 0 ps separation performance is seriously degraded and BER is degraded to 10^{-4}–10^{-3} (not shown) [28]. Such degradation is a kind of beat noise between the desired user and interference. The effect of such beat noise, termed SI beat noise in [20], has been analyzed for spectrally phase-encoded O-CDMA in [6]. As a qualitative explanation consider the following example. If the number of chips in the code is $N=100$, the broadened interference waveform intensity is ~1% of the short pulse signal peak intensity. When there is no temporal overlap, the impact of interference is very small after nonlinear processing, since the nonlinear discriminator strongly suppresses the interference signal and any remaining interference that leaks through the discriminator simply adds (in power) to the desired signal. However, when temporal overlap occurs, the optical fields (not power) sum at the input of the nonlinear device. For the prior example, the interference field amplitude is 10% of the signal field amplitude during the interval of the short pulse. Therefore, the beat-noise intensity fluctuation could be as large as ±20% (worst case) of the SI (illustrated in Fig. 10). The size of the fluctuation, which is already large, may be increased by the nonlinear optical processing—whether this is performed using an SHG device as here, using fiber-based nonlinear optical devices [7,8,19,22], or using other nonlinear devices. Such SI beat noise caused by temporal overlap is a universal problem for multiuser O-CDMA systems. Because of the coherent beat noise in multiuser O-CDMA systems, either very long code lengths, chip-synchronous transmission, or both are required when different users overlap in time; and the user count with specified BER performance is limited (therefore imposing constraints on the spectral efficiency in these systems).

2.B. Chip-Level Timing Coordination O-CDMA System

In the above slot-level timing coordination scheme using M-sequence coding, system performance is degraded as pulses overlap between users (equivalently, the time-slot duration is decreased) due to beat noise. To suppress MAI effectively, many O-CDMA systems have relied on precise timing coordination at the transmitter and/or synchronous nonlinear gating at the receiver, with coordination and synchronism required at the level of the finest feature in the coded waveforms: equal to the duration of uncoded or properly decoded pulses, typically of the order of a picosecond or below [11,12,21–25]. This is referred to as chip-level timing coordination, which requires much more stringent timing control than slot-level timing coordination since the slot

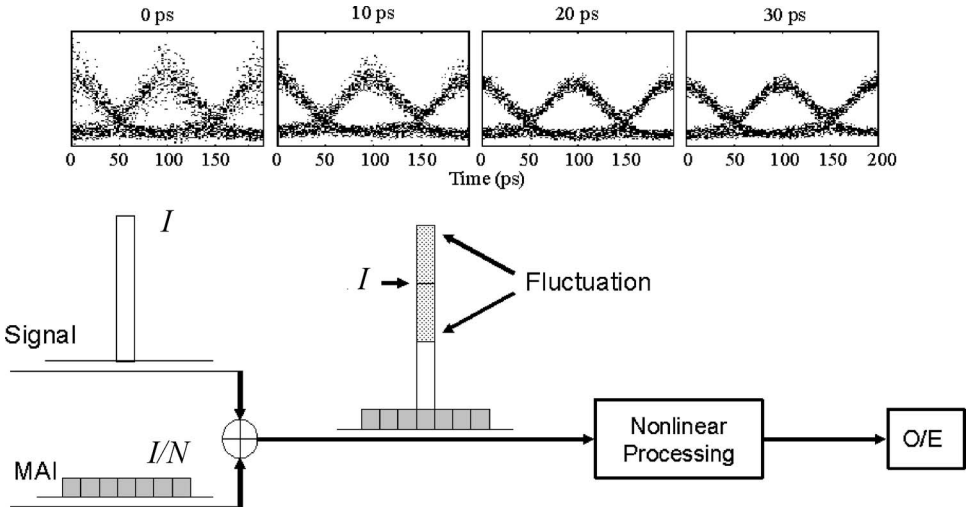

Fig. 10. Illustration of system degradation caused by pulse overlap between users. Eye diagrams of properly decoded user 1 with one interference user while tuning the user separation. Performance is degraded by the "beat noise" when two users overlap.

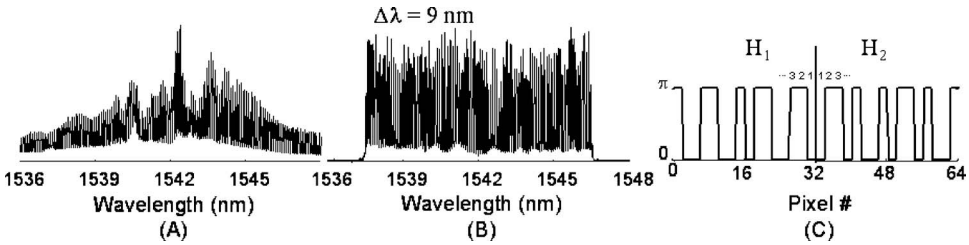

Fig. 11. (A) Spectrum before amplitude equalization. (B) Spectrum after amplitude equalization. (C) Double-Hadamard code, consisting of 16 code elements on each half of the spectrum.

duration is much longer than the chip duration. In general, increasing timing coordination and synchronism can provide greater user counts and better performance, at the cost of greater complexity. In this section, we discuss the O-CDMA system performance with increased timing control at the transmitter but still without synchronous detection at the receiver.

Considering the narrowband SHG process due to large group velocity mismatch in the PPLN waveguide, one can control the SHG yield by changing the correlation properties of the applied spectral phase code; our group has previously demonstrated as much as 30 dB MAI suppression ratio using a double-Hadamard code, showing potential for O-CDMA application [57]. In the demonstration reported here [29], we use a modified double-Hadamard coding scheme: at the transmitter each user is coded by a double-Hadamard code (H_1:H_2, $H_1 \neq H_2$) across the whole spectrum, and at the receiver it is properly decoded back to a short pulse by the same code (H_1:H_2) or improperly decoded by another code (H_3:H_4). Double-Hadamard coding requires spectral amplitude equalization, for which the SHG at the center wavelength becomes equal to the frequency correlation of the complex spectral amplitude [57]. As a result, proper sets of double Hadamard codes are fully orthogonal and ideally give zero cross talk between orthogonal codes and consequently full MAI suppression. This property remains valid in a chip-level timing coordination scheme even when pulses overlap between users.

Our experimental setup is the same as above, except the 2×128 pixel LCM array in each pulse shaper now spectrally phase codes and amplitude equalizes the spectrum of the source laser. Compared with the previous experiment, three important changes are: (1) spectral amplitude equalization, (2) chip-level timing control is introduced, and (3) the double-Hadamard coding scheme. Figure 11(A) shows the optical spectrum before amplitude equalization. Figure 11(B) shows the equalized spectrum without spectral phase coding, for which the 9 nm bandwidth covers 64 pixels of the LCM. Figure 11(C) shows one typical double-Hadamard code. We use a length-16 Hadamard code (16 code elements) on each half of the spectrum with two LCM pixels per code element. Note that the code-element order is reversed on each half of the spectrum.

Figure 12 shows the O-CDMA system results with chip-level timing coordination.

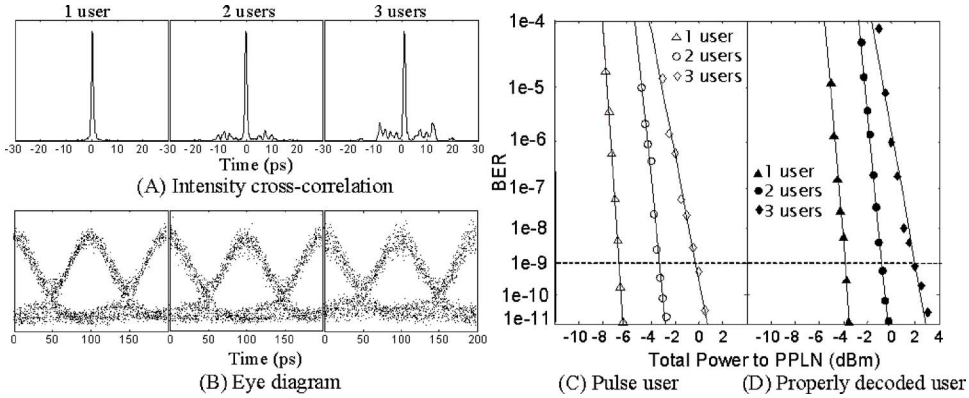

Fig. 12. Performance measurement of 10 Gbits/s O-CDMA system with chip-level timing coordination. (A) Intensity cross correlation of one, two, and three users with pulse user properly decoded. (B) Eye diagram and (C) BER measurement corresponding to (A). (D) BER measurement of one other properly decoded user.

All users are aligned at the chip-level time scale with approximately picosecond accuracy. Figure 12(A) shows intensity cross-correlation measurements in which the pulse user is properly decoded, for one user, two users, and three users. Approximately a 5 ps wide minimum occurs at the center of the interference user waveforms where the properly decoded short pulse is located, enhancing the MAI rejection. Double–length-16–Hadamard coding is used resulting in an interference user waveform broadened to ~25 ps. Figures 12(B) and 12(C) show corresponding eye diagrams and BER curves as a function of power at the nonlinear discriminator. To increase from one user to two users, the ~3.5 dB power differences between BER curves at BER=10^{-9} implies 0.5 dB power penalty due to MAI, since 3 dB arises from doubling of the number of users. Similarly, with three users a total of ~1.2 dB power penalty caused by MAI is observed at BER=10^{-9}. Figure 12(D) shows the BER curves for another properly decoded user. There is ~2.7 dB power difference compared with the pulse user shown in Fig. 12(C), mostly caused by coding degradation and coding loss [7]. This is larger than the results in Subsection 2.A due to the higher resolution used in our current pulse shapers (two pixels per code element versus four pixels per code element). Nevertheless, the BER curves in Figs. 12(C) and 12(D) show essentially similar behavior except for the power difference.

Figure 13 shows the four-user O-CDMA system results with hybrid-chip and slot-level timing coordination with the pulse user properly decoded. Figure 13(A) shows intensity cross-correlation measurements of four combinations: (a) four users separated in a time-slotted configuration; (b) overlap three MAI users, separate one desired user; (c) separate two pairs of overlapping users; (d) overlap three users including the desired user, separate one MAI user. Figures 13(B) and 13(C) show corresponding eye diagrams and BER curves, all operating at less than 3 dBm for four users (~50 fJ/bit) at BER=10^{-9}.

Considering the ~25 ps slot occupied by each user, there are four available slots for the 100 ps bit duration at 10 Gbits/s. This implies the potential of a 12-user O-CDMA system if there are three users with chip-level timing coordination within each of the four slots. In our system, the low power requirement provides substantial margin for scaling to higher bit rates and user counts while provisioning only a moderately sized optical amplifier to each receiver node, operating at practical power levels compatible with traditional optical communication systems. Although chip- and slot-level timing coordination is required in this scheme, fully asynchronous detection is achieved through the asynchronous nonlinear optical processing technique.

Although not investigated experimentally, there is potential to extend this scheme to a significantly greater number of simultaneous users. In principle, the narrowband SHG yield from a PPLN waveguide will be suppressed completely for an improperly decoded user employing a double-Hadamard code, since ideally this receiver scheme exploits the full orthogonality between users [29,57]. Ideally, double–length-16–Hadamard codes support 16 users per slot, equal to the number of orthogonal codes in the code family. Moreover, these codes can be used repeatedly in four different slots and the data in different slots can be distinguished by using a faster (40 GHz)

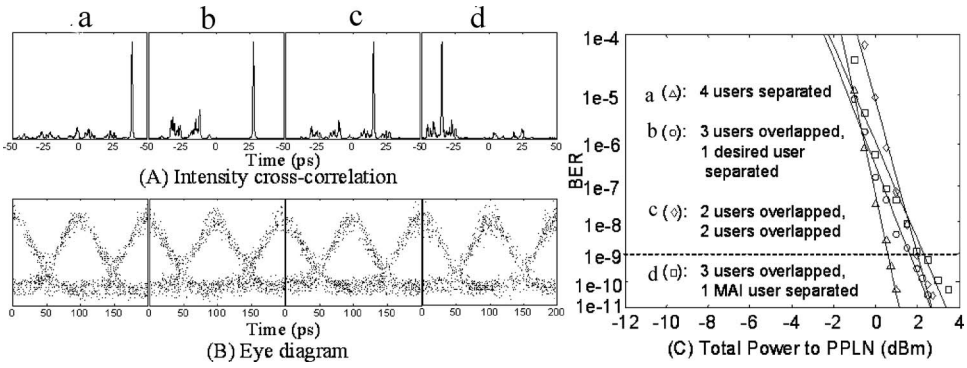

Fig. 13. Performance measurement of 4×10 Gbits/s O-CDMA system with hybrid chip- and slot-level timing coordination. (A) Intensity cross correlation of four users with pulse user properly decoded. (B) Eye diagram and (C) BER measurement corresponding to (A). a, separate four users; b, overlap three MAI users, separate one desired user; c, separate two pairs of overlapping users; d, overlap three users including desired user, separate one MAI user.

receiver. Therefore, up to 64 users are possible based on our current scheme (it can be doubled further to 128 users by polarization multiplexing). To achieve such results, a number of engineering issues would have to be carefully addressed. These include fine delay control, careful PPLN temperature control, higher precision spectral amplitude equalization, accurate spectral phase control, and careful matching between all the encoders and decoders in the system.

3. ~500 fs Pulse Transmission Over 50 km Single-mode Fiber

Ultrashort optical pulse fiber transmission plays a critical role in high-speed O-TDM systems and the O-CDMA system discussed here. However, fiber dispersion may cause serious distortion to a broadband ultrashort pulse. The most successful and widely commercialized dispersion compensation (DC) technique is the use of dispersion-compensating fiber (DCF) specially designed to have opposite dispersion parameters compared to single-mode fiber (SMF), in which most second-order and partial third-order dispersion are compensated. For ultrashort pulses, accumulated residual second- and third-order dispersion in a fiber link can still cause serious distortion even if high-quality DCF is used. Here we discuss a passive, format-independent technique capable of fine tuning and completely removing the residual dispersion for a nearly compensated fiber link, which relaxes the required precision in fiber lengths and increases the tolerance to fiber dispersion variations [40–42]. We demonstrate almost exact third-order correction for ~500 fs pulse distortion-free transmission over 50 km SMF–DCF links using a programmable pulse shaper [42]. The pulse shaper, already used for the O-CDMA encoder–decoder, functions in addition as an adjustable spectral phase equalizer allowing programmable dispersion compensation and reduces the need for careful DCF selection and precise fiber length trimming. Our results demonstrate that the pulse shaping technique can effectively remove both the residual second- and third-order dispersion for femtosecond pulse transmission in excess of 50 km without strict requirements on the DCF length, which covers the distance range of practical interest for LANs and MANs. Further, we apply the 50 km fiber transmission results in an O-CDMA system context.

The experimental setup is similar to that shown previously with the addition of SMF–DCF modules with 50 km SMF fiber between the transmitter and receiver. The spectral phase control with the pulse shaper allows dispersion control through the relation $\tau(\omega)=-(\partial\Phi(\omega)/\partial\omega)$, where $\tau(\omega)$ and $\Phi(\omega)$ are the frequency-dependent delay and spectral phase, respectively. In our system, most second-order and partial third-order dispersions are compensated by the DCF. Note that we use the commercial SMF–DCF module as is, without any effort to trim the fiber length to optimize dispersion compensation. The pulse shaper (either the pulse shaper in the encoder or decoder) is used for finely tuning dispersion. For initial experiments we use an uncoded pulse with duration 460 fs (FWHM) in the absence of the SMF–DCF modules. Figure 14 shows the details of the fine-dispersion compensation using the pulse shaper. After the SMF alone, the calculated broadening is ~5 ns. After the SMF–DCF modules, although most second-order and partial third-order dispersion is compensated, the pulse is still significantly distorted and broadened to 13.9 ps (dotted curve).

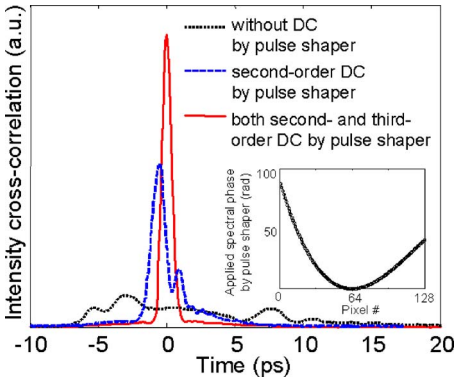

Fig. 14. Intensity cross correlation for different pulse shaper settings. Inset shows the phase profile applied by pulse shaper.

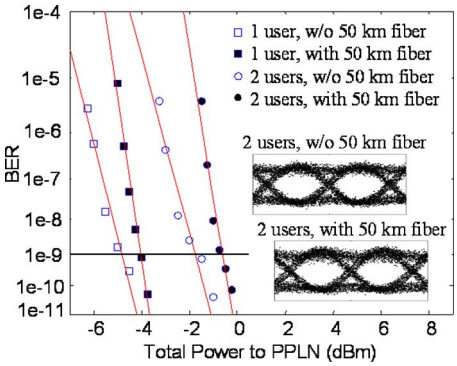

Fig. 15. BER performance for the O-CDMA system with and without 50 km fiber transmission. Insets show the eye diagrams for two users. The data modulation is 2.5 Gbits/s, where there are four pulses in each bit. After electrical filtering at receiver it shows NRZ-like eye diagrams.

If we program the pulse shaper to compensate the residual second-order dispersion only, the pulse shows an oscillating tail (dashed curve) indicative of residual third-order dispersion. If we program the pulse shaper to compensate both residual second- and third-order dispersion, the pulse is recovered back to 470 fs (solid curve), which dramatically demonstrates the capability of essentially complete dispersion compensation for sub-500 fs short pulses over 50 km of SMF by combining the techniques of DCF and a pulse shaper. The inset shows the quadratic and cubic phase profile applied by the pulse shaper to cancel the residual second- and third-order dispersion. Please note that the actual phase applied to the pulse shaper is equal to this value modulo 2π, which significantly extends the dispersion compensation range.

Now we integrate the fiber transmission technique into our O-CDMA testbed [43]. Since the spectral phase encoding and decoding is also implemented by the pulse shaper, we can overlay the function of dispersion compensation on either the encoder or decoder to simplify system implementation. Figure 15 shows a two-user O-CDMA system performance with 50 km SMF transmission (eye diagrams and BER), where a 2.5 Gbits/s PRBS $2^{23}-1$ data stream is impressed. The desired user and interference user are separated by ~50 ps in a time-slotted scheme. For both single user and two users, the power penalty at BER$=10^{-9}$ caused by 50 km fiber transmission is less than 1.3 dB. Note that we are beginning to see signs of polarization mode dispersion (PMD) even for the 50 km of SMF in our experiments [42], which likely contributes to the observed small power penalty. Although for traditional fiber systems, PMD usually attracts attention only in much longer fiber links (hundreds or thousands of kilometer fibers), for ultrashort (~500 fs) pulses used here PMD is expected to become a limit for fiber lengths significantly longer than the current 50 km range. Also note that the 2.5 Gbits/s performance here is somewhat worse than previous 10 Gbits/s system in Subsection 2.A. The data modulation is 2.5 Gbits/s, where there are four pulses in each bit. After electrical filtering at the receiver we observe non-return-to-zero (NRZ)-like eye diagrams, which is different from 10 Gbits/s return to zero (RZ) data modulation.

4. Code Translation in O-CDMA

In O-CDMA, multiple access is achieved by assigning different, minimally interfering code sequences to different transmitters, which must subsequently be detected in the presence of MAI from other users. Since multiple users share the fiber transmission medium in O-CDMA networks, a code assigned to a specific user might have already been used between certain optical nodes due to the limited code space. Code translation is a solution to resolve the conflict, in which the coded user is alternatively encoded by another unused code. As a result, code translation is an efficient way to increase user counts and/or reduce the number of required codes by reusing codes in O-CDMA networks. The ability to dynamically translate from one code to another in an O-CDMA network is analogous to dynamic wavelength conversion/switching, which is a key capability for reconfigurable wavelength division multiplexed networks [2]. Code translation in O-CDMA can be implemented via optoelectronic conversion

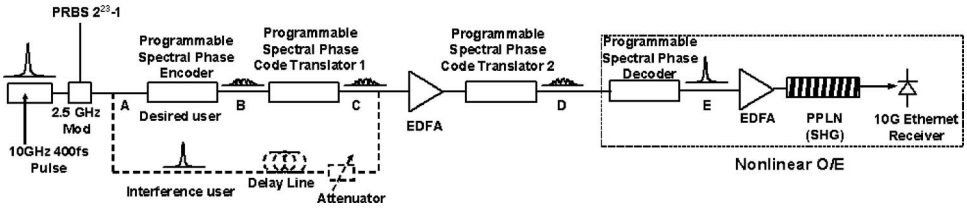

Fig. 16. Experimental apparatus for two-stage code translation.

(O/E–E/O) [44] while losing optical transparency. Previous efforts to pursue all-optical O-CDMA code translation have been reported in time-domain coding [45] and 2-D time/wavelength coding [46]. Both of these works required a complicated nonlinear optical processing scheme with short code lengths (4–8 chips) and the code translators did not support dynamic reconfiguration. Moreover, the previous work only demonstrated single-stage, single-user code translation. We have demonstrated reconfigurable all-optical code translation in our spectrally phase-coded O-CDMA testbed. We have demonstrated that both one-stage and two-stage code translations induce less than 0.9 dB power penalty for each code translation. We have also investigated multistage code translation both via simulation and by experimental emulation in a loop pulse shaper to show the potential application of our method for up to several tens of code translations [47,48]. Here we summarize the two-stage code translation results. Analogous code translation results on a high spectral efficiency, spectrally phase-coded O-CDMA system were reported subsequently in [49].

In our spectral phase-coding scheme, the code translator is the same apparatus as the O-CDMA encoder–decoder and permits multistage code translation in a simple, linear, and delay-free scheme. Code translation is essentially instantaneous, limited only by the propagation time through the free-space apparatus. Furthermore, an interference user is included in our code translation demonstration so that the effect of MAI can be evaluated, which is a key issue in any O-CDMA system demonstration.

Figure 16 shows the experimental apparatus for two-stage code translation. Four pulse shapers are connected in series, where the first shaper is an encoder, the last is a decoder, and the second and the third are code translators. The desired user is combined with an uncoded pulse interference user after the first-stage code translation. As a result, the desired user and the interference user experience different code translation paths and different numbers of code translations, emulating what would happen in an actual network environment. Optical amplifiers are added for loss compensation.

Figure 17 shows intensity cross-correlation measurements of pulse waveforms for the desired user: (A) uncoded, (B) encoded, (C) translated once, (D) translated twice, and (E) properly decoded pulses. Here instead of binary codes, the length-31 quaternary phase codes [61] are applied to the encoder, code translator 1, code translator 2, and decoder. Translated pulses remain pseudonoise waveforms but with distinct fine temporal structures. The properly decoded pulse is converted back to a short pulse, demonstrating successful two-stage code translation and decoding. Figures 17(A)–17(E) correspond to waveforms at points A–E as shown in the experiment setup of Fig. 16, but all waveforms are measured at the point E by programming unused pulse shapers to have a constant phase. The desired user and interference user (not shown) are separated by ~40 ps.

Figure 18 shows BER curves for two-stage code translation with 2.5 Gbits/s data modulation. The results without code translation are obtained by programming both code translators to have a constant phase. The results with single-code translation are

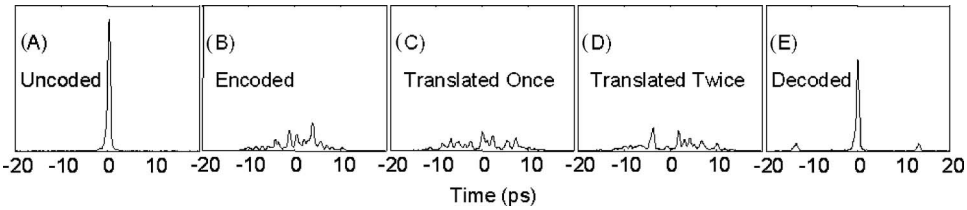

Fig. 17. Intensity cross-correlation measurements of the desired user: (A) uncoded, (B) encoded, (C) translated once, (D) translated twice, and (E) decoded pulses.

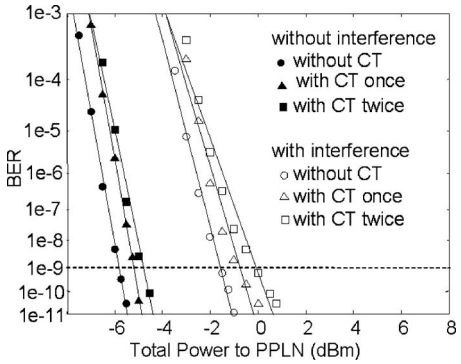

Fig. 18. BER measurements of two-stage code translation for single user and two users. CT, code translation. The data modulation is 2.5 Gbits/s, where there are four pulses in each bit.

obtained by programming code translator 2 to have a constant phase. The desired user is still properly decoded by choosing appropriate codes at the decoder for both cases. To demonstrate effective MAI suppression, results for a single user (without interference) are also shown for comparison. In both situations, less than 0.9 dB power penalty is observed at each code translation.

5. Security Issue in O-CDMA

5.A. Code-Switching Scheme

Enhanced information security is frequently mentioned as a potential advantage of O-CDMA. This is plausible at first glance considering that frequently the O-CDMA encoded signal manifests itself as a noiselike waveform that may not be accessible to an eavesdropper without knowledge of the applied code. Therefore, for a properly configured system, an eavesdropper may potentially experience a significant disadvantage in signal-to-noise ratio compared to the authorized O-CDMA receiver. However, this argument is worth deeper consideration. It has been noted [50,51] and experimentally demonstrated [27] that there is no security at all in spectrally phase-coded O-CDMA for a single-user system employing OOK. This is due to the fact that for an OOK system, although the encoded waveform is noiselike on an ultrafast time scale, it can be detected using a simple energy detector without any knowledge of the spectral code. For example, the energy detector could be a standard receiver bandwidth-limited to the bit rate that is unable to resolve the fine structure of the noiselike waveforms but integrates the energy in a bit period. As a result, although on an ultrafast time scale the noiselike coded waveform is very different from the properly decoded short pulses, it still shows a clear eye diagram, which could be detected by an eavesdropper with no knowledge of the code. Therefore, there is no security at all for such OOK single-user O-CDMA systems. On the other hand, even in a multiuser network environment, there are typically still fiber links where only a single user exists (for example, the upstream traffic in a star network as shown in Fig. 19, as pointed out by a recent systematic theoretical study on security issues in O-CDMA [50,51]). In this case eavesdropping can be easily accomplished using a simple energy detector if an OOK data modulation format is used, as pointed out above. This is also experimentally shown in the inset of Fig. 19, where there are open eye diagrams using an energy detector for both encoded and properly decoded users, despite the fact that these signals are completely different on an ultrafast time scale. References [50,51] suggest that the vulnerability to eavesdropping can be reduced for a data modulation format based on switching between two code words (in the following we refer to this as code switching or two-code keying). It is also suggested that spectral phase coding is one of the more promising approaches for O-CDMA from a security perspective, due to the large code space. Here we summarize our experimental results on this code-switching scheme for spectrally phase-coded O-CDMA.

Before going into experimental details, we would like to clarify the meaning of security in O-CDMA within the general framework of security studies in the literature. Although there are unconditionally secure systems (e.g., quantum key distribution systems), no classical communication system will ever be unconditionally secure. Most

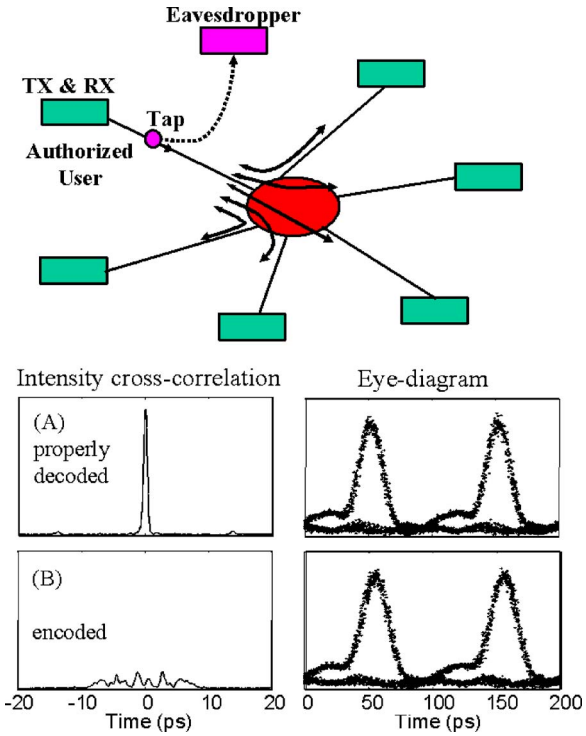

Fig. 19. Vulnerability illustration in the upstream traffic in a star network. (A) For an authorized user, a properly decoded short pulse shows a clear eye diagram. (B) For a malicious eavesdropper, encoded noiselike waveform still shows a clear eye diagram.

practical systems fall into the category of computationally secure, which is defined as requiring a sufficiently large amount of computation time and resources to break it [50,51]. The theoretical security study in [50,51] focused on determining the O-CDMA code is considered as a study of computational security in O-CDMA systems. In our work we investigate simple vulnerabilities even without searching the code space, implying that O-CDMA may not even be computationally secure.

A schematic of the code-switching scheme is shown in Fig. 20. A coupler is used to generate two arms in a complementary modulator geometry to achieve code switching.

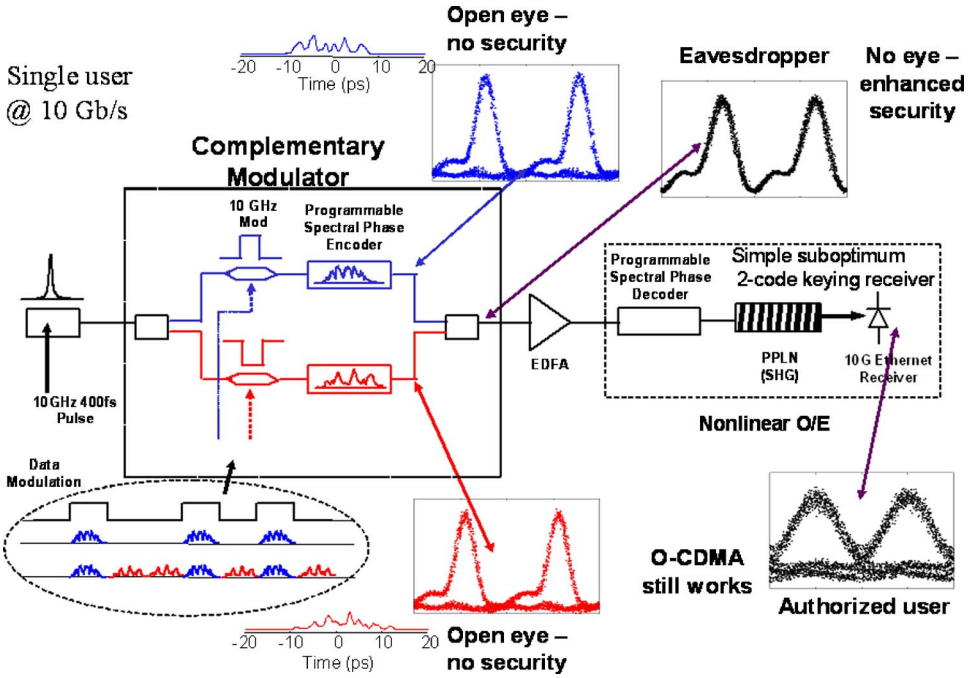

Fig. 20. Code-switching experimental setup.

Each arm is equipped with an intensity modulator employing OOK and driven by the same 10 Gbits/s PRBS data stream, but data and data bar are assigned to the two arms, respectively. The data modulated ultrashort pulses are input into fiber-coupled Fourier-transform pulse shapers to spectrally phase code the spectrum of the source laser. Two different codes (here length-31 M-sequence codes) are applied to the two arms to realize code switching. To achieve high-quality code switching, care is taken to match the average power and fiber length in each arm. After combining the two arms, bits 1 and 0 are occupied by two distinct but equal energy noiselike waveforms encoded according to codes 1 and 2, respectively. The receiver is the same as before, consisting of a decoder, a PPLN waveguide to perform the nonlinear discrimination function, and a photodiode operating at the SHG wavelength of 0.77 μm adapted from 10 Gbits/s Ethernet. For the purpose of this demonstration it is assumed that an eavesdropper could tap into the fiber link somewhere after the complementary modulator but before the decoder. We also note that fast optical-switches-based optical XOR gate has been proposed and implemented for code switching and bit-to-bit code swapping with pseudorandom swapping pattern in a recent O-CDMA security study [62].

For an eavesdropper using an energy detector, here a 20 GHz bandwidth photodiode at 1.5 μm, the eye diagram is clear for single arm (traditional single-user O-CDMA) and there is no security at all (see Fig. 20). Figure 20 also shows the detected waveforms for the code-switching scheme observed by an eavesdropper also using a simple energy detector. Now there is no eye diagram at all since both bits 1 and 0 are occupied by encoded waveforms. This demonstrates the ability to enhance security through the code-switching scheme, since information can no longer be intercepted by an eavesdropper with a simple energy detector.

On the other hand, it is important to show that the code-switching scheme still works for the authorized user using conventional O-CDMA detection: decoded by a decoder, discriminated by the PPLN, and detected by the photodiode at 0.77 μm. For the code-switching scheme, the decoder is set as code 1. After the decoder, bit 1 is properly decoded back to a short pulse to drive the PPLN to high SHG yield; while bit 0 is improperly decoded, remaining a noiselike waveform, and the SHG yield is suppressed. As a result, a clear eye diagram is observed as shown in Fig. 20. To go one step further, Fig. 21 shows the results when an interference user is added after the complementary modulator. Figure 21(A) shows the eye diagrams with an interference user modulated at 2.5 Gbits/s with OOK. The code switching user (10 Gbits/s) and interference users are separated by ~50 ps. To the eavesdropper, the data of the code-switching user is well concealed. At the authorized receiver, the code-switching data (10 Gbits/s) show a clear eye diagram after correct decoding and nonlinear processing. The authorized receiver may also choose to tune to the interference user (2.5 Gbits/s). Figure 21(B) shows the results when an unmodulated interference user at 10 GHz repetition rate is added. This emulates a code-switching interference user

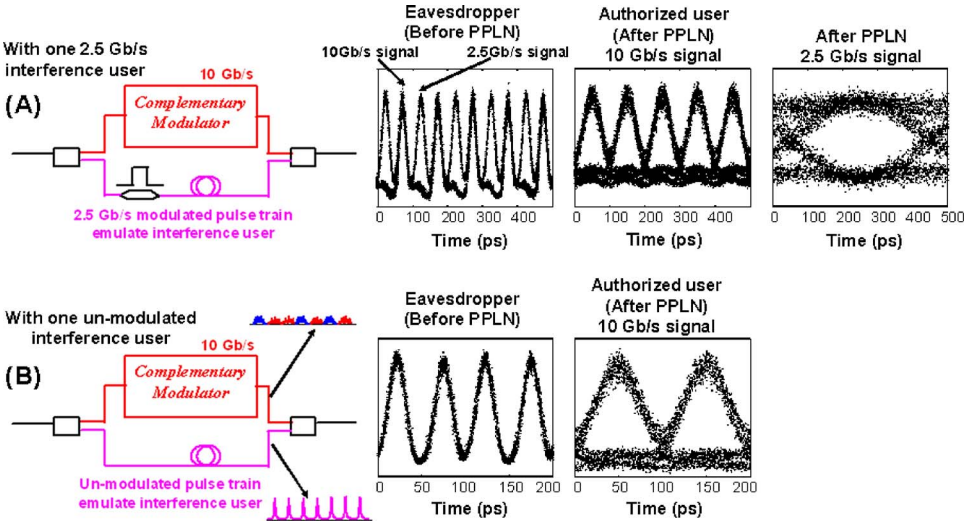

Fig. 21. Code-switching experimental setup with an interference user. (A) With one 2.5 Gbits/s data modulated interference user. A 2.5 GHz receiver is used for detecting 2.5 Gbits/s interference user. (B) With one unmodulated interference user.

in the sense that the interferer has energy during every bit period. As before the code-switching user (10 Gbits/s) and interference users are separated by ~50 ps. For the eavesdropper, the data of the code-switching user are concealed and are also indistinguishable from the interference pulse source. After proper decoding and nonlinear processing at the authorized receiver, the code-switching data (10 Gbits/s) show a clear eye diagram. The clear eye diagrams in Fig. 21 demonstrate the code-switching scheme still works for the authorized receiver using conventional O-CDMA detection, and the interference user is well suppressed.

Thus, the code-switching data modulation format enhances security compared to OOK by eliminating the vulnerability to eavesdropping based on a simple energy detector. However, this does not preclude the possibility of vulnerability to eavesdropping strategies that exploit other structures in the coding and signaling scheme. We investigate and experimentally demonstrate simple vulnerabilities, summarized here, that allow eavesdropping of data from an isolated user with code switching. These vulnerabilities allow data recovery with simple hardware and without the need for any attempt to learn the code.

First, we show a vulnerability of the code-switching scheme using a DPSK demodulator. In the code-switching scheme, bits 1 and 0 are occupied by different spectrally phase-coded waveforms. This is analogous to BPSK, where each bit has constant energy but is data coded with 0 or π phase shift for bits 0 or 1. Therefore, a simple differential phase-shift keying (DPSK) demodulator can also be used to recover data from the code-switching scheme. The DPSK format has been intensely investigated in optical fiber communication systems in recent years [63]. Briefly, the DPSK demodulator is a one-bit-delay interferometer, in which the incoming signal is split into two paths and combined again with one-bit difference between the two paths. In conventional BPSK and DPSK the signals add constructively at the interferometer output for like adjacent bits (00 or $\pi\pi$) and destructively for unlike adjacent bits (0π or $\pi 0$). This converts the phase modulation into an intensity contrast. DPSK demodulation of code-switching O-CDMA signals works in a similar way as illustrated in Fig. 22, provided that the interferometer delay is carefully matched to the data rate with precision better than the coherence time of the O-CDMA signal (usually this is the duration of the original mode-locked pulse). When adjacent bits are identical (same code waveforms), they can interfere constructively to give a high output. However, when adjacent bits correspond to different code waveforms, their interference is close to zero due to averaging over different spectral chips (assuming the usual case of code pairs with low cross correlation). Note that the recovered data is a DPSK counterpart of the original data impressed on the code-switching user. Original data can be simply recovered by using an electrical DPSK data converter. We have experimentally demonstrated this vulnerability in [53]. This DPSK vulnerability is a very serious one for several reasons. First, the eavesdropping scheme does not require any attempt to learn the O-CDMA code. Second, the eavesdropper is unaffected if the code pair used in the code-switching modulator is changed. Third, the eavesdropper is able to exploit the full energy in the intercepted signal, as opposed to other schemes where only the energy per code chip can be exploited [50,51]. Given that the eavesdropper is able to use a conventional high-sensitivity detector requiring only a few femtojoules per bit, while the O-CDMA receiver requires nonlinear processing (demonstrated down to 30 fJ per bit, which is still an order of magnitude higher than conventional lightwave receivers), there is a significant likelihood that the eavesdropper can attain signal-to-noise ratio comparable with or even better than that of the O-CDMA receiver. Clearly,

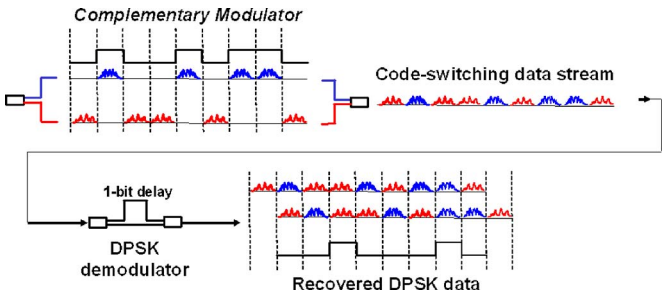

Fig. 22. Vulnerability illustration of the code-switching scheme using a DPSK demodulator.

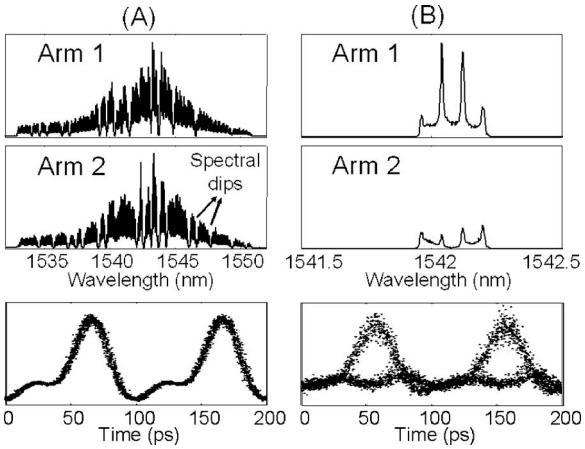

Fig. 23. Spectra of coded arm 1 and coded arm 2, and waveform of the combined signals measured by photodetector and sampling scope. (A) Whole spectra, (B) spectra with dip filtered by a narrow bandpass filter in the vicinity of 1542 nm.

this fails to fulfill the premise for security in O-CDMA, which is that the eavesdropper without knowledge of the code should be at a signal-to-noise ratio disadvantage.

Now we focus on another vulnerability of the code-switching scheme arising from coding-induced spectral dips (phase-to-amplitude conversion) that allow eavesdropping with a receiver consisting only of a tunable optical filter and a simple energy detector. As we already discussed, for the code-switching scheme there is no eye diagram at all with such a simple energy detector since both bits 1 and 0 are occupied by encoded waveforms, as shown in Fig. 23(A). In this sense the security is enhanced since the information is concealed by the code-switching scheme to resist simple interception from a malicious eavesdropper. However, for spectrally phase-coded O-CDMA the coding process will generate spectral dips, as discussed earlier in connection with Fig. 7. In the current experiment dips are clearly visible in the spectra of Fig. 23(A), where the coded spectra of the two arms are measured individually by blocking the opposite arm of the code-switching transmitter. This dip phenomenon results from diffraction effects experienced by frequency components falling at transitions in the spectral phase code and is expected for fundamental reasons explained quantitatively in [7,60]. Each spectral dip identifies a phase transition in the spectrum; one can easily recover the codes from the measured spectra according to this principle. Here we show that the spectral dips lead to structure in the signals that can be exploited directly for eavesdropping in a simple way. For the code-switching scheme, clear spectral measurements for individual arms become somewhat difficult since two differently coded spectra are combined together. However, one can recover the data by simply scanning a narrow bandpass optical filter across the combined spectra even without measuring the code. At the spectral positions where one arm has a dip while the other arm does not, there is a power difference between them. Such power difference will generate eye diagrams, which is similar to an OOK signal from a single arm. Figure 23(B) shows such an example. In the vicinity of 1542 nm there is no dip for arm 1 but a dip for arm 2 on the coded spectra as shown in Fig. 23(A). We use a high-resolution pulse shaper [64] as a tunable narrow bandpass filter to achieve this discrimination, where four spectral lines (separated at 10 GHz: the repetition rate) are filtered out. As expected, an eye diagram shown in Fig. 23(B), which demonstrates a very clear vulnerability to eavesdropping.

5.B. Multiuser Aggregation

Another simple and intuitive way to enhance security in O-CDMA is to aggregate multiple users with a desired user: these aggregated users behave like interference users and make it more difficult for an eavesdropper to isolate an individual O-CDMA channel. In this section, we investigate security issues in O-CDMA with aggregation. Figure 24 shows the experimental setup and concept illustration of multiuser aggregation in O-CDMA. This is similar to a multiuser O-CDMA system but with the assumption that multiple data channels are combined in a single transmitter that is in a secure location. In our experiments pulses are data loaded with an intensity

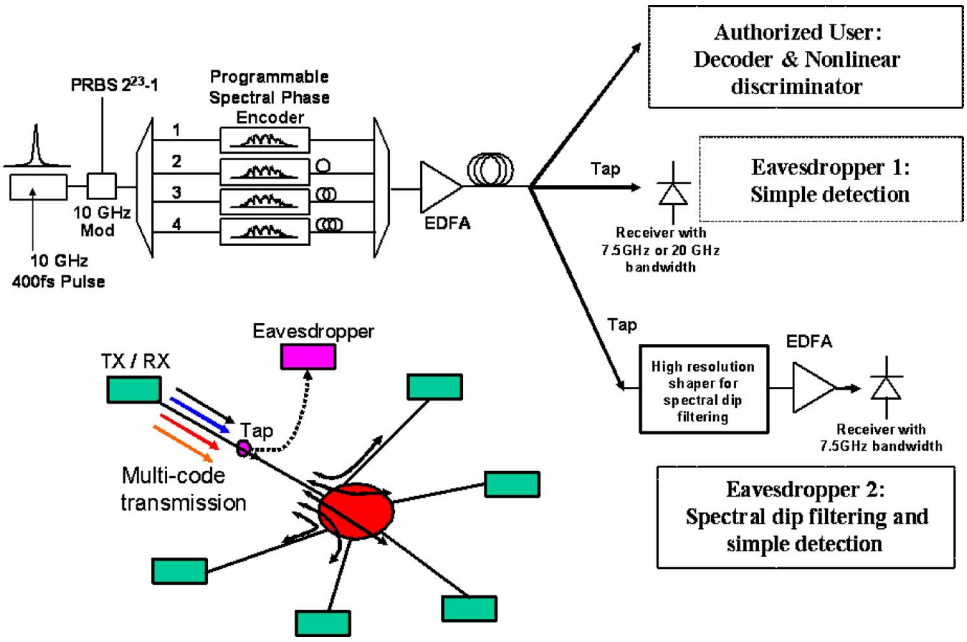

Fig. 24. Experimental setup and concept illustration of multiuser aggregation in O-CDMA.

modulator employing OOK driven by a 10 Gbits/s PRBS $2^{23}-1$ data stream. A 1×4 coupler is used to generate up to four users, where 1 is the desired user while 2, 3, and/or 4 are aggregated users. At an authorized O-CDMA receiver with knowledge of the codes, a desired data channel can be recovered by employing the identical O-CDMA detection scheme as described in Section 2.

First, we investigated security issues in an aggregated O-CDMA system with time slotting: all of the channels are temporally separated. Figure 25 shows the eye diagrams for two-user aggregation (i.e., one desired user and one aggregated user) for different delays (measured by a 7.5 GHz receiver). For the delays between 50 and 20 ps, the eye diagrams are clear and have open structure for the desired user, which means that the data of the desired user can be recovered (lack of security) by assigning an appropriate sampling point. Below 20 ps separation the data is concealed (security is enhanced) because coded users overlap with each other in time. Even then some information is available to the eavesdropper, who can easily detect when both channels are sending data 0, for example. We also implemented experiments for time-slotted O-CDMA with three- and four-user aggregation in an attempt to enhance the security level. Figure 26 shows eye diagrams for the time-slotted O-CDMA system with three- and four-user aggregation. All users are assigned to one of four slots in the 100 ps

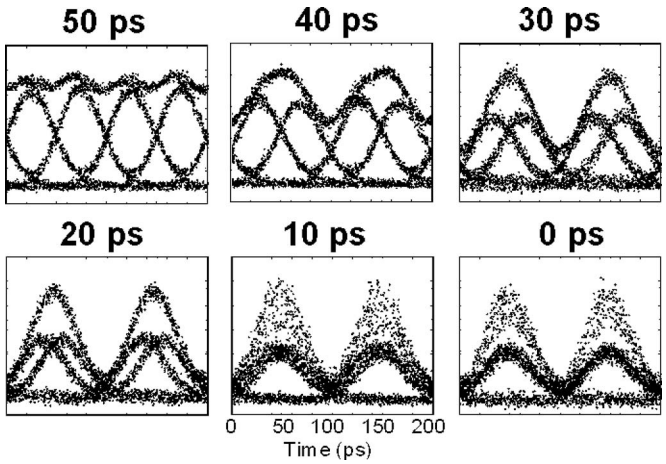

Fig. 25. Eye diagrams for time-slotted O-CDMA system with two-user aggregation. The receiver is 7.5 GHz bandwidth.

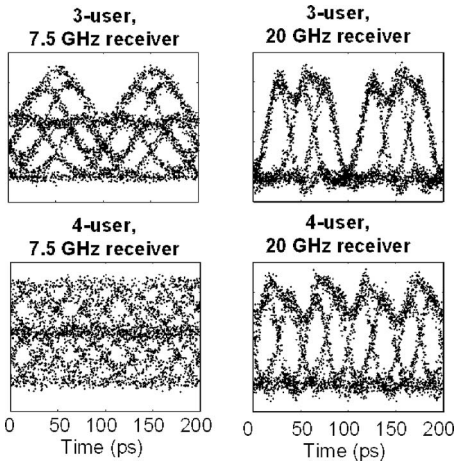

Fig. 26. Eye diagrams for time-slotted three- and four-user aggregation. The receiver is 7.5 or 20 GHz bandwidth.

data period. Using a 7.5 GHz receiver, the time-slotted O-CDMA system may enhance security since it is difficult to get a clear open eye for an individual channel. But this security can easily be cracked by using a slightly larger receiver bandwidth. As shown in Fig. 26, a 20 GHz receiver is sufficient to resolve a clear open eyes for both three- and four-user aggregation.

Since a time-slotted O-CDMA system is vulnerable, in the following experiments we overlap all the users in time, as per Fig. 25 in the zero-delay case. However, other vulnerabilities may still exist. Similar to the code-switching scheme, one possibility is to exploit structure in the coded waveforms, such as the spectral dips in spectrally phase-coded O-CDMA. To investigate this, a high-resolution line-by-line pulse shaper is again used for narrowband spectral dip filtering and the eye diagrams are measured as shown in Fig. 27. For one user only (in this case the user has no dip at the possible spectral dip position), it shows a clear eye diagram as expected. For two-user aggregation, we put the filter at a position where one user (either desired or aggregated user) has a dip while the other does not. Then, very similar to our experiment on spectral dip filtering in the code-switching scheme (Fig. 23), we are able to detect a recognizable eye diagram due to the power contrast at dips position. For three-user aggregation, we put the filter at a position where two users have dips while the other one user does not. The eye diagram is still recognizable (though noisy), which indicates some vulnerability even for three-user aggregation. For four-user aggregation (not shown), the eye diagram is almost completely closed (even for the narrowband filter tuned to a position where the three interfering users have spectral dips). It is clear that the beat noise (caused by residual power in the dips) degrades the eye diagrams with more users. For two-user aggregation, the BER after spectral dip filtering for two-user aggregation typically can be pushed down to 10^{-6} after optimizing the bandwidth and center wavelength of the narrow bandpass filter. In terms of security, such a level of BER may be sufficiently secure for some purposes, but inadequately secure for many others (for example, an uncompressed video data stream). For more user aggregation, it may provide some security against the eavesdropping using spectral dip filtering since the eye diagram and BER performances after spectral dip filtering are poor.

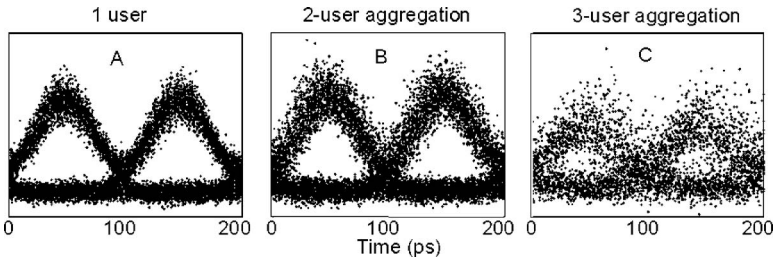

Fig. 27. Eye diagram after spectral dip filtering. (A) One user, (B) two-user aggregation, (C) three-user aggregation.

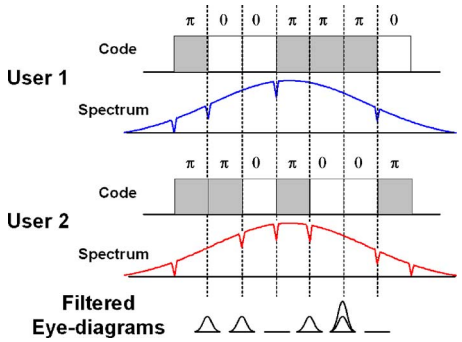

Fig. 28. Concept illustration to tap code in two-user aggregation O-CDMA scheme by spectral dip filtering.

For two-user aggregation, in addition to the vulnerability as evidenced by the eye diagrams after spectral dip filtering shown in Fig. 27(B), we further demonstrate that it is possible to scan the spectral dips to determine the individual O-CDMA codes for both of the overlapped users. Figure 28 illustrates our strategy to determine the codes by spectral dip filtering in the case of two-user aggregation. By filtering each dip position, one at a time, we can readily determine whether (1) both users have dips, which results ideally in a one-level eye (a bottom rail), (2) neither user has a dip, which results ideally in a three-level eye (a midrail as well as a top rail), or (3) there is a dip for one user but no dip for the other user, which results ideally in a two-level eye (a top and bottom rail). In cases (1) we know that both users have a phase transition at the examined spectral position, while in case (2) we know that neither user has a phase transition. In case (3) we know that one and only one user has a phase transition, but we do not know which user to assign it to. Therefore, only case (3) requires further investigation. For case (3), our strategy is to set the eavesdropper's spectral filter (high-resolution pulse shaper) to simultaneously select two such dip positions (in each dip position, one and only one user has a dip). Now the task becomes to determine if the two dips both belong to the same user or if they come from different users. This task is accomplished by noting that when the two dips come from the same user, ideally we expect a two-level eye; while if the two dips come from different users we expect a three-level eye. Once all this dip information has been gained, one can easily recover the codes since each spectral dip marks a $0-\pi$ phase transition.

To demonstrate this code-tapping idea, we perform simple experiments in which we take the spectrum directly from the mode-locked laser (without pulse compression), which is coded with a seven-chip code. Desired user and aggregated user are coded with different seven-chip codes. Note that we tap the codes blindly (that is, someone else sets the codes and we do not know them beforehand). As shown in Fig. 29, for the seven-chip code there are only six potential dip positions that need to be examined under single-dip filtering (the spectra are measured after tapping the codes by blocking either the desired user or aggregated user). The output of the single-dip filter displays either one-, two-, or three-level eyes as expected although the clarity of the eyes is degraded by beat noise. To unambiguously distinguish between these eyes, histograms are also plotted, where the intensity data points between −15 and 15 ps are placed into 80 equally spaced bins. By counting the number of peaks in the histograms, it is straightforward to determine the numbers of levels in the eye diagram. From these results we determine that both users had dips (hence phase transitions) at spectral locations 3 and 6 and that neither had a dip (or a phase transition) at spectral location 5. The remaining spectral locations have only one dip among the two users; hence measurements in which pairs of these spectral locations are examined together are performed in order to assign each dip to a specific user. As shown in Fig. 30, the data for selection (dips 1 and 2) and (dips 2 and 4) contain sufficient information to fully assign the dips and recover the codes for both users. In particular, these data show that dips 2 and 4 belong to the same user, while dip 1 belongs to the other user. If we assign dips 2 and 4 to user 2 (this assumption is not important since it does not matter which code belongs to which user), the code for user 1 is $[\pi\ 0\ 0\ \pi\ \pi\ \pi\ 0]$ and the code for user 2 is $[\pi\ \pi\ 0\ \pi\ 0\ 0\ \pi]$. This is the same as the actual codes (see Fig. 29). If the first chip starts from 0 instead of π, then the code

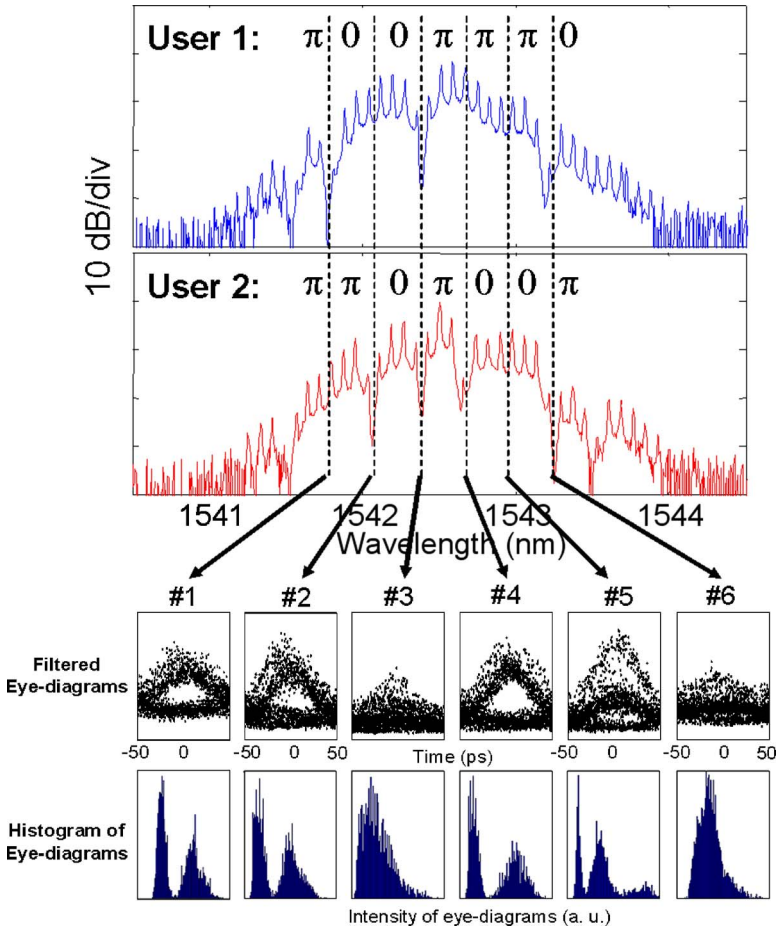

Fig. 29. Code tapping by spectral dip filtering in two-user aggregation scheme: single-dip filtering.

simply has an overall phase shift of π, which is unimportant. The additional data from selecting the pair (dips 1 and 4) does not contain new information but can be used for a consistency check.

Finally, we note that the spectral dip vulnerabilities discussed above can be masked by a modified phase-coding scheme in which a dip is intentionally placed at every spectral location corresponding to the transition location between two code chips [53]. Nevertheless, a key conclusion of our work is that structure in coded O-CDMA signals may potentially be exploited in order to eavesdrop, with relatively simple equipment

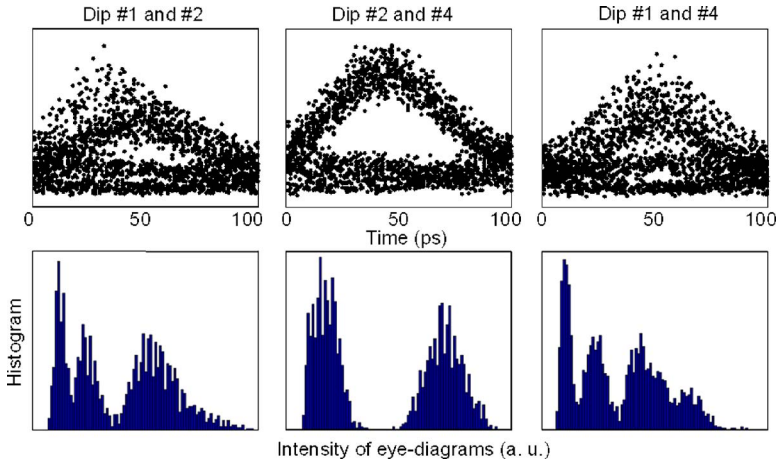

Fig. 30. Code tapping by spectral dip filtering in two-user aggregation scheme: two-dip filtering.

and both in single-user and aggregated-user scenarios. Although we have focused our investigation on spectral phase coding, it is likely that other O-CDMA schemes suffer from analogous vulnerabilities based on their structure. Therefore, one must exercise great care in assessing and mitigating such vulnerabilities if the security features of O-CDMA are of interest.

6. Summary

In this paper we have first given a general discussion of O-CDMA research. We have then reviewed recent progress in our spectrally phase-coded O-CDMA system including 10 Gbits/s multiuser system demonstrations, essentially distortionless ultrafast fiber transmission over 50 km single-mode fiber with ~500 fs pulses, code translation demonstrations as may be required in a multipoint network implementation, and experimental studies of potential security issues in O-CDMA. In parallel with efforts from many other O-CDMA groups worldwide, it is clear that O-CDMA remains of significant research interest in the community, especially for applications in optical access networks, and is stimulating development of interesting optical signal processing technologies. However, there are still challenges, among which we emphasize (1) the need to reduce the complexity and cost of the entire system, including the broadband laser source, encoding–decoding devices, detection system, and simplified timing control for multiuser O-CDMA systems; and (2) the need to further improve the system performance of multiuser O-CDMA systems, including increasing the user count and total capacity while maintaining error-free operation for all users.

Acknowledgments

The authors thank R. V. Roussev, C. Langrock, and M. M. Fejer for providing the PPLN device and D. S. Seo and S.-D. Yang for their help in experiments. This work was supported in part by the Defense Advanced Research Projects Agency (DARPA) under Space and Navel Warfare (SPAWAR) Systems Center San Diego contract N66001-06-1-2028. Any opinions, findings, and conclusions or recommendations expressed in this publication are those of the authors and do not necessarily reflect the views of DARPA and SPAWAR.

References and Links

1. I. P. Kaminow and T. L. Koch, eds., *Optical Fiber Telecommunications*, (Academic, 1997), Vol. III.
2. I. P. Kaminow and T. Y. Li, eds., *Optical Fiber Telecommunications*, (Academic, 2002), Vol. IV.
3. J. Shah, "Optical CDMA," Opt. Photonics News **14**, 42–47 (2003).
4. P. R. Prucnal, M. A. Santoro, and T. R. Fan, "Spread spectrum fiber-optic local area network using optical processing," J. Lightwave Technol. **4**, 547–554 (1986).
5. A. M. Weiner, J. P. Heritage, and J. A. Salehi, "Encoding and decoding of femtosecond pulses," Opt. Lett. **13**, 300–302 (1988).
6. J. A. Salehi, A. M. Weiner, and J. P. Heritage, "Coherent ultrashort light pulse code-division multiple access communication systems," J. Lightwave Technol. **8**, 478–491 (1990).
7. H. P. Sardesai, C.-C. Chang, and A. M. Weiner, "A femtosecond code division multiple access communication system test-bed," J. Lightwave Technol. **16**, 1953–1964 (1998).
8. S. Shen, A. M. Weiner, G. D. Sucha, and M. L. Stock, "Bit error rate performance of ultrashort-pulse optical CDMA detection under multi-access interference," Electron. Lett. **36**, 1795–1797 (2000).
9. R. Papannareddy and A. M. Weiner, "Performance comparison of coherent ultrashort light pulse and incoherent broad-band CDMA systems," IEEE Photon. Technol. Lett. **11**, 1683–1685 (1999).
10. H. Tsuda, H. Takenouchi, T. Ishii, K. Okamoto, T. Goh, K. Sato, A. Hirano, T. Kurokawa, and C. Amano, "Spectral encoding and decoding of 10 Gbit/s femtosecond pulses using high resolution arrayed-waveguide grating," Electron. Lett. **35**, 1186–1188 (1999).
11. H. Sotobayashi, W. Chujo, and K. Kitayama, "1.6-b/s/Hz 6.4-Tb/s QPSK-OCDMA/WDM (4 OCDMA×40 WDM×40 Gb/s) transmission experiment using optical hard thresholding," IEEE Photon. Technol. Lett. **14**, 555–557 (2002).
12. H. Sotobayashi, W. Chujo, and K. Kitayama, "Highly spectral-efficient optical code-division multiplexing transmission system," IEEE J. Sel. Top. Quantum Electron. **10**, 250–258 (2004).
13. P. Petropoulos, N. Wada, P. C. Teh, M. Ibsen, W. Chujo, K. Kitayama, and D. J. Richardson, "Demonstration of a 64-chip OCDMA system using superstructured fiber gratings and time-gating detection," IEEE Photon. Technol. Lett. **13**, 1239–1241 (2001).

14. C. S. Bres, I. Glesk, and P. R. Prucnal, "Demonstration of an eight-user 115-Gchip/s incoherent OCDMA system using supercontinuum generation and optical time gating," IEEE Photon. Technol. Lett. **18**, 889–891 (2006).
15. P. Saghari, P. Kamath, V. R. Arbab, M. Haghi, A. E. Willner, J. A. Bannister, and J. D. Touch, "Experimental demonstration of an interference-avoidance-based protocol for O-CDMA networks," in *Optical Fiber Communication Conference*, 2006 Technical Digest Series (Optical Society of America, 2006), paper PDP46.
16. J. E. McGeehan, S. M. Reza, M. Nezam, P. Saghari, A. E. Willner, R. Omrani, and P. V. Kumar, "Experimental demonstration of OCDMA transmission using a three-dimensional (time-wavelength-polarization) codeset," J. Lightwave Technol. **23**, 3282–3289 (2005).
17. X. Wang, N. Wada, T. Hamanaka, K. Kitayama, and A. Nishiki, "10-user, truly-asynchronous OCDMA experiment with 511-chip SSFBG en-decoder and SC-based optical thresholder," in *Optical Fiber Communication Conference*, 2005 Technical Digest Series (Optical Society of America, 2005), paper PDP33.
18. T. Hamanaka, X. Wang, N. Wada, and K. Kitayama, "511-chip SSFBG and DFG-based optical thresholder enabled compound data rate (10 Gbps ~ 622 Mbps) OCDMA experiment for multiple service provisioning platform," in *Optical Fiber Communication Conference*, 2006 Technical Digest Series (Optical Society of America, 2006), paper OThT4.
19. X. Wang, T. Hamanaka, N. Wada, and K. Kitayama, "Dispertion-flattened-fiber based optical thresholder for multiple-access-interference suppression in OCDMA system," Opt. Express **13**, 5499–5505 (2005).
20. X. Wang and K. Kitayama, "Analysis of beat noise in coherent and incoherent time-spreading OCDMA," J. Lightwave Technol. **22**, 2226–2235 (2004).
21. V. J. Hernandez, W. Cong, R. P. Scott, C. Yang, N. K. Fontaine, B. H. Kolner, J. P. Heritage, and S. J. B. Yoo, "320-Gb/s capacity (32 users × 10 Gb/s) SPECTS O-CDMA local area network testbed," in *Optical Fiber Communication Conference*, 2006 Technical Digest Series (Optical Society of America, 2006), paper PDP45.
22. R. P. Scott, W. Cong, K. B. Li, V. J. Hernandez, B. H. Kolner, J. P. Heritage, and S. J. B. Yoo, "Demonstration of an error-free 4 × 10 Gb/s multiuser SPECTS O-CDMA network testbed," IEEE Photon. Technol. Lett. **16**, 2186–2188 (2004).
23. W. Cong, C. X. Yang, R. P. Scott, V. J. Hernandez, N. K. Fontaine, B. H. Kolner, J. P. Heritage, and S. J. B. Yoo, "Demonstration of 160- and 320-Gb/s SPECTS O-CDMA network testbeds," IEEE Photon. Technol. Lett. **18**, 1567–1569 (2006).
24. A. Agarwal, P. Toliver, R. Menendez, S. Etemad, J. Jackel, J. Young, T. Banwell, B. E. Little, S. T. Chu, J. Hryniewicz, W. Chen, W. Chen, and P. J. Delfyett, "Fully programmable ring resonator based integrated photonic circuit for phase coherent applications," in *Optical Fiber Communication Conference*, 2005 Technical Digest Series (Optical Society of America, 2005), paper PDP6.
25. A. Agarwal, P. Toliver, R. Menendez, T. Banwell, J. Jackel, and S. Etemad, "Spectrally efficient six-user coherent OCDMA system using reconfigurable integrated ring resonator circuits," IEEE Photon. Technol. Lett. **18**, 1952–1954 (2006).
26. Z. Jiang, D. S. Seo, S.-D. Yang, D. E. Leaird, A. M. Weiner, R. V. Roussev, C. Langrock, and M. M. Fejer, "Four user, 2.5 Gb/s, spectrally coded O-CDMA system demonstration using low power nonlinear processing," in *Optical Fiber Communication Conference*, 2004 Technical Digest Series (Optical Society of America, 2004), paper PDP29.
27. Z. Jiang, D. S. Seo, S.-D. Yang, D. E. Leaird, A. M. Weiner, R. V. Roussev, C. Langrock, and M. M. Fejer, "Four user, 2.5 Gb/s, spectrally coded O-CDMA system demonstration using low power nonlinear processing," J. Lightwave Technol. **23**, 143–158 (2005).
28. Z. Jiang, D. S. Seo, S.-D. Yang, D. E. Leaird, A. M. Weiner, R. V. Roussev, C. Langrock, and M. M. Fejer, "Four user, 10 Gb/s spectrally phase coded O-CDMA system operating at ~30 fJ/bit," IEEE Photon. Technol. Lett. **17**, 705–707 (2005).
29. Z. Jiang, D. S. Seo, D. E. Leaird, A. M. Weiner, R. V. Roussev, C. Langrock, and M. M. Fejer, "Multi-user, 10 Gb/s spectrally phase coded O-CDMA system with hybrid chip and slot-level timing coordination," IEICE Electron. Express **1**, 398–403 (2004).
30. R. L. Peterson, R. E. Ziemer, and D. E. Borth, *Introduction to Spread-Spectrum Communications* (Prentice Hall, 1995).
31. J. G. Proakis, *Digital Communications*, 3rd ed. (McGraw-Hill, 1995).
32. X. Wang, N. Wada, T. Miyazaki, G. Cincotti, and K. Kitayama, "Field trial of 3-WDM × 10-OCDMA × 10.71 Gbps, truly-asynchronous, WDM/DPSK-OCDMA using hybrid E/D without FEC and optical threshold," in *Optical Fiber Communication Conference*, 2006 Technical Digest Series (Optical Society of America, 2006), paper PDP44.
33. X. Wang, N. Wada, G. Cincotti, T. Miyazaki, and K. Kitayama, "Demonstration of over 128 Gbps-capacity (12-user × 10.71 Gbps/user), asynchronous OCDMA using FEC and AWG-based multi-port optical encoder/decoders," IEEE Photon. Technol. Lett. **18**, 1603–1605 (2006).
34. D. E. Leaird, S. Shen, A. M. Weiner, A. Sugita, S. Kamei, M. Ishii, and K. Okamoto, "Generation of high-repetition-rate WDM pulse trains from an arrayed-waveguide grating," IEEE Photon. Technol. Lett. **13**, 221–223 (2001).
35. D. E. Leaird, A. M. Weiner, S. Shen, A. Sugita, S. Kamei, M. Ishii, and K. Okamoto, "High repetition rate femtosecond WDM pulse generation using direct space-to-time pulse shapers and arrayed waveguide gratings," Opt. Quantum Electron. **33**, 811–826 (2001).
36. D. E. Leaird, A. M. Weiner, S. Kamei, M. Ishii, A. Sugita, and K. Okamoto, "Generation of flat-topped 500-GHz pulse bursts using loss engineered arrayed waveguide gratings," IEEE Photon. Technol. Lett. **14**, 816–818 (2002).

37. S. Kawanishi, "Ultrahigh-speed optical time-division-multiplexed transmission technology based on optical signal processing," IEEE J. Quantum Electron. **34**, 2064–2079 (1998).
38. E. Yoshida, T. Yamamoto, A. Sahara, and M. Nakazawa, "320 Gbit/s TDM transmission over 120 km using 400 fs pulse train," Electron. Lett. **34**, 1004–1005 (1998).
39. T. Yamamoto and M. Nakazawa, "Third- and fourth-order active dispersion compensation with a phase modulator in a terabit-per-second optical time-division multiplexed transmission," Opt. Lett. **26**, 647–649 (2001).
40. C.-C. Chang, H. P. Sardesai, and A. M. Weiner, "Dispersion-free fiber transmission for femtosecond pulses using a dispersion-compensating fiber and a programmable pulse shaper," Opt. Lett. **23**, 283–285 (1998).
41. S. Shen and A. M. Weiner, "Complete dispersion compensation for 400-fs pulse transmission over 10-km fiber link using dispersion compensating fiber and spectral phase equalizer," IEEE Photon. Technol. Lett. **11**, 827–829 (1999).
42. Z. Jiang, S.-D. Yang, D. E. Leaird, and A. M. Weiner, "Fully dispersion compensated ~500 fs pulse transmission over 50 km single mode fiber," Opt. Lett. **30**, 1449–1451 (2005).
43. Z. Jiang, S.-D. Yang, D. E. Leaird, A. M. Weiner, R. V. Roussev, C. Langrock, and M. M. Fejer, "Fully dispersion compensated ~500 fs pulse transmission over 50 km SMF and application to ultrafast O-CDMA," in *Conference on Lasers and Electro-optics*, 2005 Technical Digest Series (Optical Society of America, 2005), paper CFK2.
44. K. Kitayama, "Code division multiplexing lightwave networks based upon optical code conversion," IEEE J. Sel. Areas Commun. **16**, 1309–1319 (1998).
45. K. Kitayama, N. Wada, and H. Sotobayashi, "Architectural considerations for photonic IP router based upon optical code correlation," J. Lightwave Technol. **18**, 1834–1844 (2000).
46. D. Gurkan, S. Kumar, A. Sahin, A. Willner, K. Parameswaran, M. Fejer, D. Starodubov, J. Bannister, P. Kamath, and J. Touch, "All-optical wavelength and time 2-D code converter for dynamically-reconfigurable O-CDMA networks using a PPLN waveguide," in *Optical Fiber Communication Conference*, 2003 Technical Digest Series (Optical Society of America, 2003), paper FD6.
47. Z. Jiang, D. S. Seo, D. E. Leaird, A. M. Weiner, R. V. Roussev, C. Langrock, and M. M. Fejer, "Reconfigurable all-optical code translation in spectrally phase coded O-CDMA networks," J. Lightwave Technol. **23**, 1979–1990 (2005).
48. D. S. Seo, Z. Jiang, D. E. Leaird, and A. M. Weiner, "Pulse shaper in a loop: demonstration of cascadable ultrafast all optical code translation," Opt. Lett. **29**, 1864–1866 (2004).
49. R. C. Menendez, P. Toliver, S. Galli, A. Agarwal, T. Banwell, J. Jackel, J. Young, and S. Etemad, "Network applications of cascaded passive code translation for WDM-compatible spectrally phase-encoded optical CDMA," J. Lightwave Technol. **23**, 3219–3231 (2005).
50. T. H. Shake, "Security performance of optical CDMA against eavesdropping," J. Lightwave Technol. **23**, 655–670 (2005).
51. T. H. Shake, "Confidentiality performance of spectral-phase-encoded optical CDMA," J. Lightwave Technol. **23**, 1652–1663 (2005).
52. D. E. Leaird, Z. Jiang, and A. M. Weiner, "Experimental investigation of security issues in OCDMA: a code-switching scheme," Electron. Lett. **41**, 817–819 (2005).
53. Z. Jiang, D. E. Leaird, and A. M. Weiner, "Experimental investigation of security issues in O-CDMA," J. Lightwave Technol. **24**, 4228–4234 (2006).
54. B. B. Wu, P. R. Prucnal, and E. E. Narimanov, "Secure transmission over an existing public WDM lightwave network," IEEE Photon. Technol. Lett. **18**, 1870–1872 (2006).
55. A. M. Weiner, "Femtosecond pulse shaping using spatial light modulators," Rev. Sci. Instrum. **71**, 1929–1960 (2000).
56. K. R. Parameswaran, R. K. Route, J. R. Kurz, R. V. Roussev, M. M. Fejer, and M. Fujimura, "Highly efficient second-harmonic generation in buried waveguides formed by annealed and reverse proton exchange in periodically poled lithium niobate," Opt. Lett. **27**, 179–181 (2002).
57. Z. Zheng and A. M. Weiner, "Spectral phase correlation of coded femtosecond pulses by second-harmonic generation in thick nonlinear crystals," Opt. Lett. **25**, 984–986 (2000).
58. Z. Zheng, A. M. Weiner, K. R. Parameswaran, M. H. Chou, and M. M. Fejer, "Low power spectral phase correlator using periodically poled $LiNbO_3$ waveguides," IEEE Photon. Technol. Lett. **4**, 376–378 (2001).
59. Z. Jiang, D. S. Seo, S.-D. Yang, D. E. Leaird, A. M. Weiner, R. V. Roussev, C. Langrock, and M. M. Fejer, "Low power, high-contrast coded waveform discrimination at 10 GHz via nonlinear processing," IEEE Photon. Technol. Lett. **16**, 1778–1780 (2004).
60. R. N. Thurston, J. P. Heritage, A. M. Weiner, and W. J. Tomlinson, "Analysis of picosecond pulse shape synthesis by spectral masking in a grating pulse compressor," IEEE J. Quantum Electron. **22**, 682–696 (1986).
61. S. Boztas, R. Hammons, and P. V. Kumar, "4-phase sequences with near-optimum correlation properties," IEEE Trans. Inf. Theory **38**, 1101–1113 (1992).
62. I. Glesk, Y.-K. Huang, C.-S. Brès, and P. R. Prucnal, "OCDMA platform for avionics application," Electron. Lett. **42**, 1115–1116 (2006).
63. A. H. Gnauck and P. J. Winzer, "Optical phase-shift-keyed transmission," J. Lightwave Technol. **23**, 115–130 (2005).
64. Z. Jiang, D. S. Seo, D. E. Leaird, and A. M. Weiner, "Spectral line-by-line pulse shaping," Opt. Lett. **30**, 1557–1559 (2005).